Title	Development of Bearingless Motor with Rectifier Circuit
Author(s)	Chen, Li
Citation	高知工科大学，博士論文.
Date of issue	2007-03
URL	http://hdl.handle.net/10173/590
Rights	
Text version	author

Development of Bearingless Motor with Rectifier Circuit

Chen Li

A dissertation submitted to
Kochi University of Technology
in partial fulfillment of the requirements
for the degree of

Doctor of Philosophy

Special Course for International Students
Department of Engineering
Graduate School of Engineering
Kochi University of Technology
Kochi, Japan

March 2007

Abstract

Bearingless motor mechanism has functions of both a magnetic bearing and a motor. It is therefore able to suspend the rotor and generate torque simultaneously. The development of bearingless motor has attracted considerable attention in recent years. One of the reasons is that bearingless motor has no physical contact with the spinning rotor, which will contribute to longer motor life, negligible friction loss, no wear, higher speed and no need of complex lubrication system for extreme environment. The second reason is that properly designed bearingless motor can be operated in a wide range of temperatures, and it can lead to a reduction in vibrations as well.

Bearingless motors can be used to artificial hearts, high speed drives, and generators.

In this thesis, a new type of bearingless motor with a rectifier circuit is proposed. The feature of the proposed bearingless motor is that there is a rectifier in the rotor winding, which ensures the induced current to flow in a fixed direction. Therefore, the magnetized rotor will hold the characteristics of permanent magnet. The proposed motor is supposed to work just like a bearingless permanent magnet (PM) stepping motor, which possesses the advantages such as no demagnetization, less rotor reluctance and higher mechanical strength. It is suitable to work at high-speed high temperature circumstances.

The objective of this research work is focused on the development of the bearingless motor with a rectified rotor. The study has been carried out by means of numerical simulation, finite element method (FEM) analysis and experiments. At the beginning, the feasibility for the proposed bearingless motor is verified by numerical simulation, and simple experiments have validated the simulation results preliminary. After that, a test machine prototype I is fabricated, and practical experiment is conducted to analyze the characteristics of the motor. But it is found that the rotor cannot rotate as we supposed like a stepping motor. FEM analysis results show that there are zero torque positions for this prototype. Based on the FEM analysis results, prototype II is designed and fabricated, which overcomes the deficiency of zero torque position. For this prototype, it is verified that sufficient enough levitation force and rotation torque can be

produced by means of both FEM and experiments. Furthermore, the strategy about how to realize the radial force and rotation torque control is studied by FEM. So far, the rotor levitation has been implemented after trials of experiments.

***Index Terms**:* **Bearingless motor, FEM analysis, Rectifier circuit coil, Radial force, Torque.**

Contents

Chapter 1 Introduction

1.1 Background

1.1.1 What bearingless motor is

In conventional motors, the rotor is supported by two radial mechanical bearings. The physical contact between the rotor and mechanical bearing will inevitably cause friction, wear and power losses, which confined the rotational speed and positioning accuracy. Besides, the friction for the contacting will cause noise.

Active magnetic bearing (AMB) uses actively controlled electromagnetic forces to control the motion of a rotor or other ferromagnetic body in air. Magnetic bearings are a no-contacting technology. Contact-free suspension leads to important advantages relative to conventional rolling bearings: negligible friction loss and no wear, higher reliability, low-maintenance, and higher speeds in extreme environments without requiring complex lubrication systems, and it can restrain the vibration and noise.

Typically, in an active magnetic bearing (AMB) system, the rotating force driving the shaft is provided by other mechanisms such as a motor. Such a configuration results in a relatively long shaft, which decreases the system critical speeds, and in turn complicates the control task.

Bearingless motor is an innovation which possesses the capabilities of both a magnetic bearing and a motor. It is therefore able to suspend the rotor and generate torque simultaneously. Sometimes it is also called self-bearing motor or integrated motor-bearing. Besides all the advantages a magnetic bearing has, the shaft of bearingless motor is shorter than that of a motor or magnetic bearing, therefore, higher operating speeds are possible. Furthermore, a bearingless motor has fewer components with respect to a magnetic bearing system, so the reduction of cost is possible.

There are some special fields such as bioreactors and semiconductor-technology, which require maintenance-free, long lifetime and sterile. Bearingless motor can meet all of these requirements. Bearingless motor can be used to artificial hearts [67], respiratory support equipment, flywheel drive and generators, satellite reaction wheel, momentum wheels; food process, pharmacy process, information storage drives, which are suitable work in harsh environments as low temperature, high temperature, vacuum, poisonous gas atmospheres.

The major challenge in this technology lies in the design of a control device and algorithm that coordinates the radial forces without interfering with the function of the motor.

However there are several drawbacks associated with bearingless motors in comparison with conventional motors. The fact is that stator performs two functions, namely levitation and rotation, which may result in the limited current capacity of the windings and magnetic flux density saturation, that is, the performance of motor may be limited. Other drawbacks include eddy current losses and complicated control system. These disadvantages, however, can be outweighed by the advantages that bearingless motor possessed.

1.1.2 History of bearingless machines

In 1842, Earnshaw proved that a stable three-axis magnetic suspension system couldn't be achieved using only passive permanent magnets. According to Earnshaw's theorem, to ensure stability, at least one axis must be actively controlled [1]. After the World War II, the development of magnetic levitated systems was greatly accelerated by the advancement of electrical technologies. Subsequently, several research teams were involved in developing actively controlled magnetic suspension systems for various applications. Due to the enormous progress achieved in electronics, the number of industrial applications of active magnetic bearing technology has been considerably increased. The applications include high-speed centrifuges, vacuum pumps, machine tool spindles, medical devices, robotics, non-contact actuators. These and other applications are described in [2-11]. A brief historical review of magnetic bearings can

be found in [12].

In the mid of 1970's, the integration of motor with magnetic bearing was proposed by Hermann [13, 14], who put forward the primitive electro magnet with p and p+2 stator windings. And Meinke [15] proposed a split winding motor. But at that time, inverter was very expensive, and there was little idea in application of digital signal processors (DSP) and field oriented control theories. In addition, for digital control system, the sampling frequency was slow, so the system stability was difficult to be guaranteed.

The associated technologies with beaingless machines were matured in the mid of 1980s, and a number of bearingless system structures were proposed. After that, based on the vector control theory, the configurations of stator winding and pole numbers were studied.

In 1985, Higuchi [16] proposed a stepping motor integrated with magnetic bearing structure. The motor includes a decoupling structure of torque and radial force taking advantage of motor exciting current.

In 1988, a disk type motor with axial force control by adjusting the exciting motor current was proposed [17]. And from the late 1980's to the early 1990's, field oriented control method [18,19] started to be used, and a basic structure for the stator winding with 4 and 2 poles was adopted [18,20-23].

1.1.3 Related technologies

For the bearingless machines, the controller will control the output coil currents to produce a rotating magnetic field, and at the same time control the rotor displacement and rotation flux strength, generating the desired radial force to realize the rotor levitation and rotation. In order to realize the precise and stable control, feedback control strategy is necessary, and the processing speed of controller must be fast enough to meet the requirement of sampling speed. The rapid development of the related technologies contributed to the realization of bearingless machines. The associated technologies are given in Fig.1.1 [24]. They are:

1. Vector control theory for rotating electromagnetic machines can be used to control the instantaneous magnetic flux.

2. High speed digital signal processing technology

3. High speed high precision inverter technology with low cost power electronics

4. The development of magnetic bearing and suspension technology

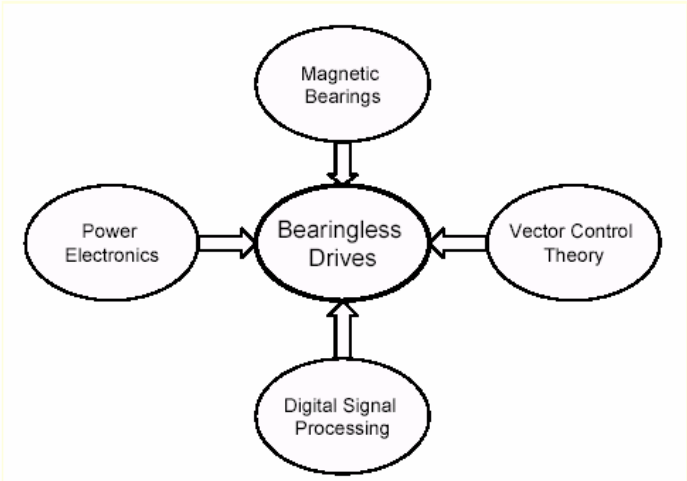

Fig. 1. 1 Related technologies

1.1.4 Bearingless motor structures

Since bearingless motors have so many advantages and special applications, so far, various types of self-bearingless motors, which functionally combine motor with magnetic bearing, have been developed. Bearingless motor technology offers many mechanical and electrical design variants for different kinds of applications.

A. Types of bearingless motor

Recently, a variety of bearingless motors--including permanent magnet, induction, and reluctance motors were introduced. These motors have different characteristics and different suitable applications. Among them, induction motor [23,25-38] is adopted widely for industrial applications because of their advantages such as simple configuration, good reliability, and low price. But the low efficiency in light-load conditions restricts their applications in some fields.

Switched-reluctance motors will be good candidates for the electric propulsion system because they have inherent fault-tolerance and rotor robustness at high rotational speeds (no coil windings on the rotor). In addition, this type of motor generates a high

radial force in the air gap that might be able to be used for rotor levitation (bearing function) [39,40].

From the point of view of quantities of the developed bearingless motors, permanent magnet bearingless motor is becoming the greatly investigated for the sake of increasing efficiency [41-51] and compactness.

Permanent magnet bearingless motors are divided into three categories based on the rotor structures. One is surface mounted permanent magnet (SPM) rotor (see Fig.1.2.), another is interior permanent magnet (IPM) rotor, and the last is buried permanent magnet (BPM) rotor.

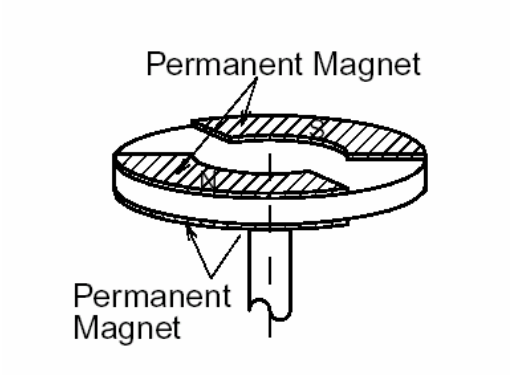

Fig. 1. 2 Surface mounted permanent magnet rotor

The SPM motor is that PMs are glued or bound to the surface of a rotor iron. The IPM motors have square-shaped holes in laminated silicon steel. The PMs are inserted and fixed in the holes. Some IPM motors need nonmagnetic shaft. For the BPM rotor, PMs are near the rotor surface just like SPM motors, but the PMs are inserted in holes in laminated silicon steel.

As far as the rotor design for torque and radial force generation is concerned, thick PMs with large air gap contribute to produce a large torque; however, thin PMs with small air-gap are preferred in radial force generation because of the low resistances. In comparison with the electromagnetic motor, permanent magnet bearingless motor is more effective even with a relatively large air gap; it is helpful to reduce the motor volume. However, for permanent magnet, there are also some disadvantages, such as demagnetization and limited mechanical strength [52].

There are a number of reports on synchronous reluctance [53-55] and homopolar

bearingless motor [56,57] as well.

For homopolar, synchronous reluctance and switched reluctance motors, the rotors are made of silicon iron, and the air gap is small, therefore, the magnetic resistance in radial force flux path is low.

B. Stator winding configurations

As far as the stator winding configuration is concerned, a representative one is the 4 poles motor winding and 2 poles radial force winding structure, and the radial forces can be regulated to any desired directions by adjusting the air gap flux distribution [18, 58, 59]. This stator configuration is valid for both cylindrical rotor and salient pole rotors. It is also easy to exchange winding functions in cylindrical rotor. This configuration contributes to the magnetic field decoupling of rotation torque and radial force.

There are still many reports about p-pole and p+2 poles configuration [42,43,60].

About the split winding, the mid point of 3-phase windings is connected to a neutral point, and then independent current regulators are used to drive the 6 terminals. The current values are adjusted to supply original motor current with slight variations to produce radial force.

Similar concepts can be applied to motors with concentrated windings. These windings are very practical in small power motors.

It is also noted that a reduction of the number of windings is reported in a single-phase motor with well-adjusted controllers [45,46,61,62].

In addition, there are a good number of reports on bearingless motors with special mechanical structure, such as sliced motor [63,64], disk type rotor [65,66], outer rotor [67-69] and ring type rotor. The sliced motor is a radial motor with a short axial length, and the rotor is stable with only 2 axes active control. The disk type motor generates axial magnetic force basically. The outer rotor has a rotating outside part for saving space for blood pump application. And the ring type rotor has a hole inside the rotor to accommodate water blades.

1.2 Motivation

The development of bearingless motor has attracted considerable attention in the lately years. One of the reasons is that bearingless motor has no physical contact with the spinning rotor, thus the friction which usually exists in conventional motors has been eliminated. The absence of friction not only contributes to longer motor life but also elimination of the need for lubrication. Because lubrication often causes problems in vacuum and other sterilized environments. The second reason is that properly designed bearingless motor can be operated in a wide range of temperatures, and often leads to a reduction in vibrations.

In comparison of electromagnetic with permanent magnetic motor designs, it can be concluded that in small motor applications, permanent magnet contributes to reduce the motor volume and to increase the motor efficiency considerably. Especially in applications with large air gaps, other design strategies cannot be competed with it. But there are some disadvantages for permanent magnet. For example, the mechanical strength of permanent magnet is limited, and under the situation of high temperature, ferromagnetic material will lose its permanent magnetism. Therefore, permanent magnet motor is not suitable for high speed and high temperature situations.

For a switched reluctance motor (SRM), it has many good performance, such as robustness, high efficiency, low cost, high speed, simple structure, easy to maintain, high torque in low speed, simple power converter circuits with reduced number of switches, excellent controllability and smaller dimension of the motor in comparison to the other motors [70,71]. Although it has been known for a long time, SRM has not been very often utilized because of acoustic noise that comes from torque dip and detection of rotor position [72]. SRM has been started to be used with the development of power electronic devices. However, SRM still preserves the excessive torque ripple problem, especially in the variable speed applications [75,76]. The main reason of this problem is the stepping nature of the motor, which causes undesired effect on bearing system and makes acoustic noise, although the emission of acoustic noise is a characteristic of all electric motors.

Based on these considerations, a new type of bearingless motor that has the merits of

both permanent magnet and switch reluctance bearingless motor is proposed.

1.3 Objectives and Dissertation Structure

The objective of this research work is to develop the new type of bearingless motor with rectifier circuit including the design, feasibility study and practical verification.

This thesis contains three themes, firstly, the numerical analysis for the proposed rectifier bearingless motor structure is conducted, then according to the FEM analyses, the optimal mechanical structure of the prototype is determined; finally to realize the rotor levitation and rotation by experiments.

The design process is as follows: firstly, an analytical study using linear analysis methods is conducted, and the feasibility is verified preliminary; then experiments are carried out, some variable relationships such as radial force versus air gap, radial force with the control current and exciting current, flux density among air gap versus control current are studied. The results, on one hand, validate the feasibility, and on the other hand, give a direction for the improvement of prototype structure. Finally, based on the Finite Element Method (FEM) analyses and experiment results, a modified prototype is built, and the rotor levitation and rotation are realized.

The thesis is organized as follows: First, the principle of proposed bearingless motor with rectifier circuits is given in Chapter 2. The numerical analysis for feasibility investigation and simple experiment results are presented in Chapter 3. In Chapter 4 and Chapter 5, the FEM analyses and modified prototype are introduced, respectively. And the experimental evaluation for rotor levitation and rotation are presented in Chapter 6. Finally, concluding remarks are given in Chapter 7.

Chapter 2 Proposal of Bearingless Motor with Rectifier Circuit

2.1 Introduction

Permanent magnet bearingless motors hold some advantages such as small volume and higher efficiency. However, permanent magnet has limited mechanical strength, and demagnetization under the situation of high temperature. Therefore, permanent magnet motor is not suitable for high speed and high temperature situations.

In order to take advantage of the merits and overcome the deficiencies of permanent magnet, a new type of beaingless motor with rectifier circuit is proposed.

The proposed bearlingless motor structure is using a rotor with rectifier circuit coil to replace the permanent magnet rotor, and it is supposed to work just like a bearingless PM stepping motor. Therefore, the proposed bearingless motor will inherit all the performances of permanent magnet motor. Additionally, the rotor has a better mechanical strength compared with permanent magnet motor, since the material of rotor is silicon steel sheet, and the reluctance can be decreased. Furthermore, it can overcome the deficiency of demagnetization. Properly designed bearingless motor can be operated in a wide range of temperatures, and the vibration can be restricted.

2.2 Principle of Bearingless Motor with Rectifier Circuit

The configuration schematic of rectified bearingless motor is shown in Fig.2.1. It consists of an eight- pole stator and a four-pole rotor. There are two sets of coils on the stator, in which one set of coils are connected with the diametrically opposite stator coil in series, and AC current is applied to this coil, they are called exciting coils; the other

set of coils can be controlled separately, DC current is applied to these coils to control the generation of rotor torque and radial force, they are called control coils. In addition, there is one set of coil wound on the rotor poles in series, and a rectifier diode is connected in the rotor winding circuit. Therefore when AC current is applied to the exciting coil, DC current will be induced in the rotor windings owing to the existence of the rectifier diode, which makes the magnified rotor poles hold a fixed polarity and work just like a permanent magnet.

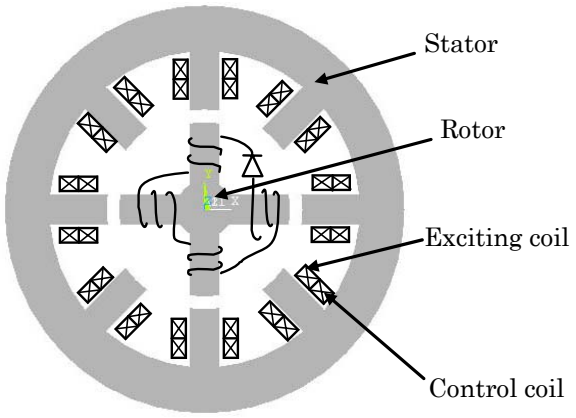

Fig.2. 1 Configuration of rectified bearingless motor

2.3 How to Make Virtual Permanent Magnet

Firstly, just one phase is taken to by analyzed. The schematic of the stator and rectified rotor is shown in Fig.2.2, which will be used to explain how the silicon iron sheet rotor can possess the characteristic of permanent magnet.

Just as Fig. 2.2 shows, one set of stator coil is connected with the opposite stator coil in series. These coils are excited by AC current and called as exciting coils. Another set of coils are called as control coils, the control coil current is used to control rotation torque and radial force, the magnitude and direction of torque and radial forces can be adjusted by regulating the control current. In addition, one set of coils is wound on the rotor poles in series, and a rectifier diode is connected to the rotor winding circuit. Therefore, when AC current is applied to the exciting coils, DC current will be induced in the rotor windings owing to the existence of the rectifier diode. This guarantees the

magnetic flux of rotor to flow in a fixed direction, therefore, the rotor will keep a fixed polarity, and can work just like a permanent magnet.

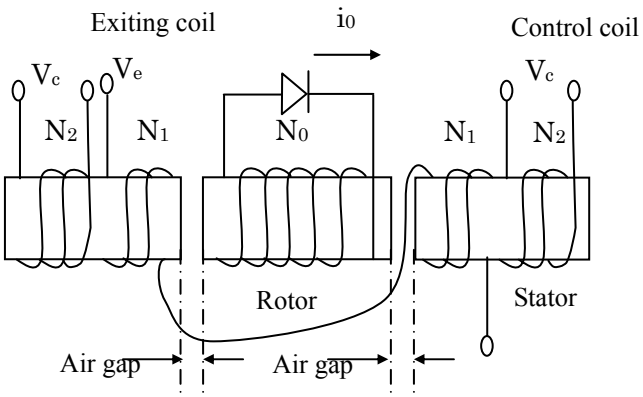

Fig.2. 2 The schematic of rectified rotor and stator

2.4 Summary and Remarks

In this chapter, the principle of the proposed bearingless motor with rectifier circuit is introduced. The feature of the proposed motor configuration is that a rectifier circuit is connected to the rotor winding, therefore, the magnetized rotor functionally possess the characteristic of permanent magnet. In comparison with permanent magnet, this structure can overcome mechanical strength deficiency and high temperature demagnetization of permanent magnet.

Chapter 3 Modeling and Simulation on 1DOF Rectifier Circuit

3.1 Feasibility Analyses by Numerical Simulation

For the proposed bearingless motor with rectifier circuit, the feasibility investigation is conducted by numerical simulation. Firstly, attentions are focused on a two-pole motor. For the symmetrical structure of the motor, the analyses presented here can be readily extended to a multi-pole motor.

The schematic of stators and rectified rotor is shown in Fig.3.1, which is used to verify that the rectified rotor can hold the characteristic of permanent magnet. For the structure shown in Fig.3.1, the air-gap length g is much smaller than the dimensions of the section area of rotor and stator. Therefore, the magnetic flux ϕ will follow the path

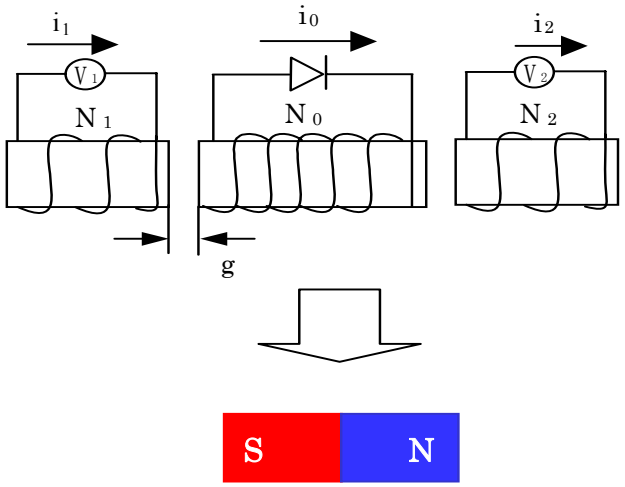

Fig.3. 1 Schematic of rotor with rectified rotor

defined by the core and the air gap, and the techniques of magnetic circuit analysis can be used.

In Fig.3.1, N_0, N_1 and N_2 are the turn numbers of rotor and stator coils respectively. v_1 and v_2 are the exciting voltages applied to the stator coils; v_0 is the induced electromotive force (EMF) in the rotor coil, g is the air gap. The terminal-voltage expressions of stator and rotor can be expressed as follows

$$v_0 = r_0 i_0 + \frac{d\phi_0}{dt} \tag{3.1}$$

$$v_1 = r_1 i_1 + \frac{d\phi_1}{dt} \tag{3.2}$$

$$v_2 = r_2 i_2 + \frac{d\phi_2}{dt} \tag{3.3}$$

where ϕ_0, ϕ_1 and ϕ_2 are the magnetic flux linkages flowing through the rotor and stator coils; r_0, r_1 and r_2 are the resistances of rotor and stator coils respectively; i_0 is the induced current in rotor coil, i_1 and i_2 are the exciting currents in stator coils; L_0, L_1 and L_2 are self inductances of rotor and stator coils respectively.

Magnetic flux linkages ϕ_0, ϕ_1 and ϕ_2 can be respectively expressed as

$$\phi_0 = L_0 i_0 + M_1 i_1 + M_2 i_2 \tag{3.4}$$

$$\phi_1 = L_1 i_1 + M_1 i_0 + M_{12} i_2 \tag{3.5}$$

$$\phi_2 = L_2 i_2 + M_2 i_0 + M_{12} i_1 \tag{3.6}$$

where M_1, M_2 and M_{12} are mutual inductances between rotor and stators.

Therefore, when the exciting voltages applied to the exciting stator coils are

$$v_1 = v_2 = A_m \sin \omega t \tag{3.7}$$

in which A_m is the amplitude of the input voltage, and ω is the input voltage frequency, the simulation results are shown in Fig.4.2.

From Fig.3.2, it can be seen that when AC current is applied to the exciting stator coil, DC current is induced in the rotor coil, and the exited rotor flux linkage almost keeps constant. This verified that the magnetized rotor could work just like a permanent

magnet.

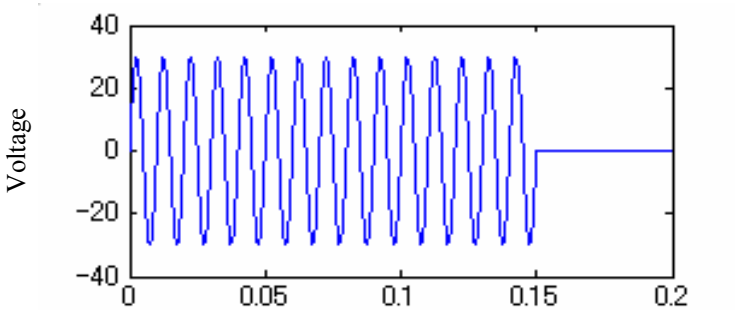

Exiting voltage

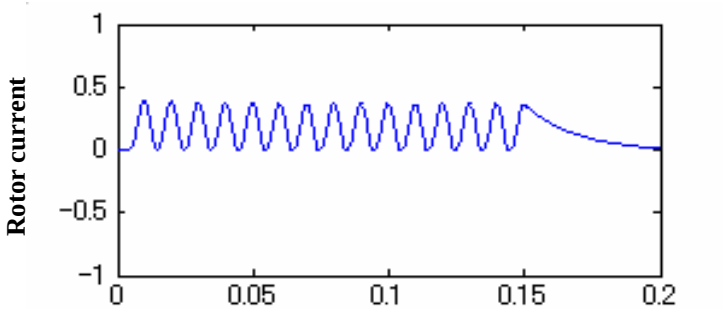

Induced current in rotor coil

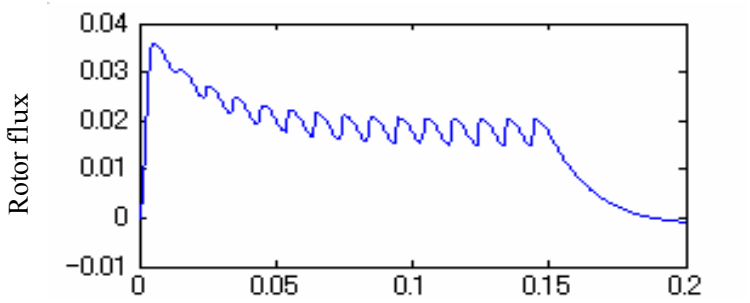

Flux linkage of rotor

Fig.3. 2 Simulation results

3.2 Experimental Studies on 1DOF Analyses

3.2.1 Rotor can work just like a permanent magnet

In order to verify the feasibility of bearingless motor with rectifier circuit, a simple experiment is carried out at the beginning, the structure of the test instrument is shown in Fig.4.3, which is merely 1 degree of freedom (DOF) instrument.

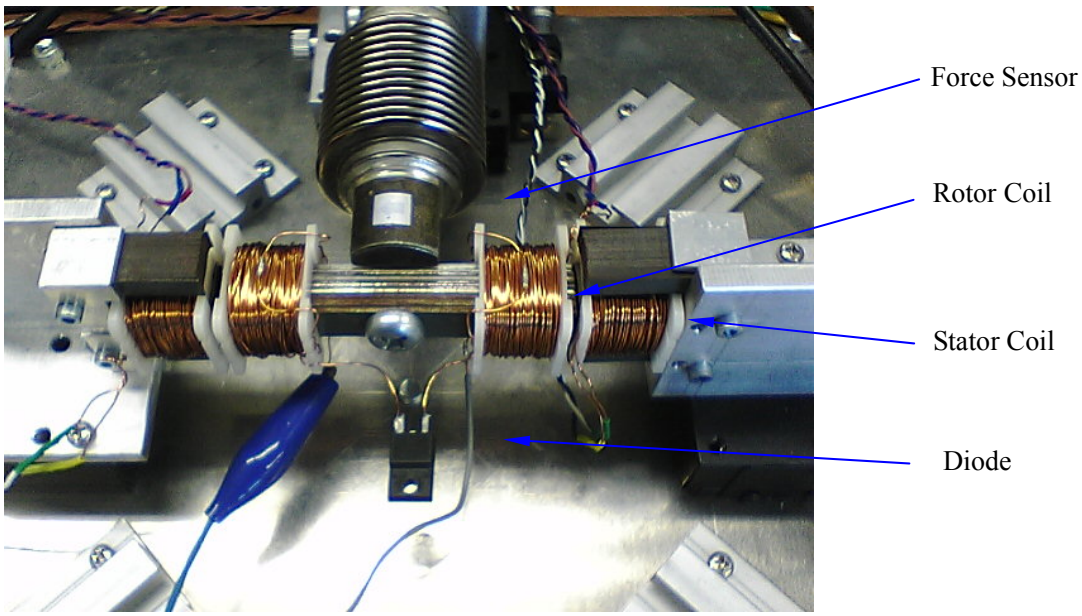

Fig.3. 3 Test instrument of rotor with rectifier circuit

The test instrument shown in Fig.3.3 is composed of stators, and rotor with rectifier circuit. The stator coils are connected with the opposite stator coil in series, and AC current is applied to this coil; the rotor coils are connected in series too, and there is a diode in the rotor coil circuit. The turn numbers of exciting stator coil and the rotor coil is 100 and 200, respectively.. The structure of the test instrument is the same as shown in Fig.2.2.

Using this test instrument, AC voltage is applied to the stator-exciting coil, and the induced current is measured by oscilloscope (TDS3014B), the results are shown in

Fig.3.4, Fig.3.5 and Fig.3.6.

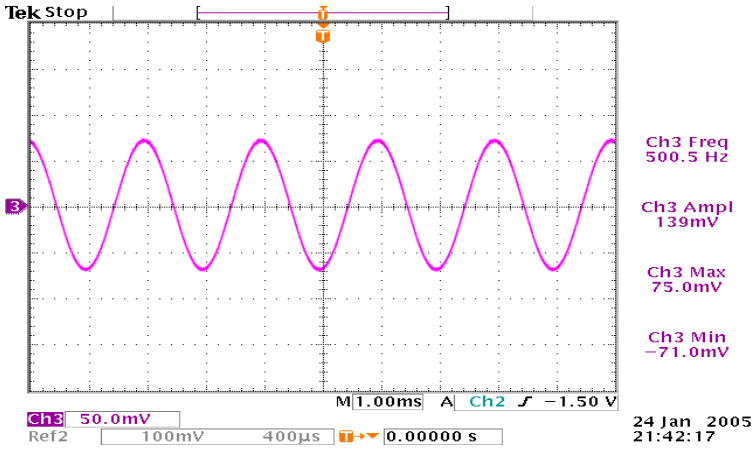

Fig.3. 4 Applied voltage

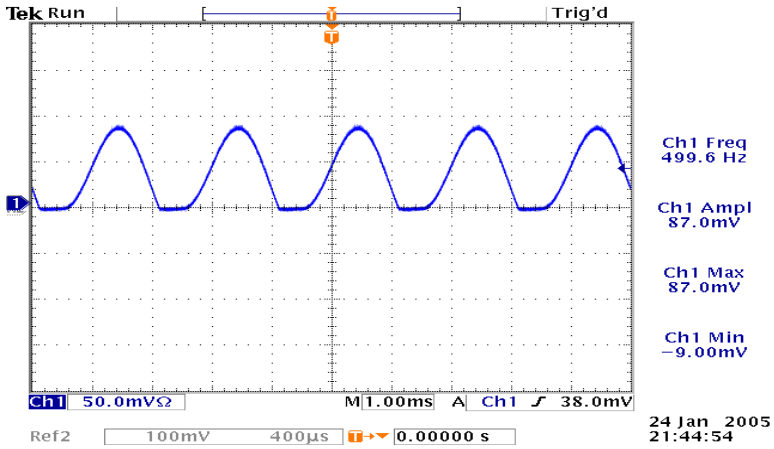

Fig.3. 5 Waveform of induced current with diode in the rotor coil

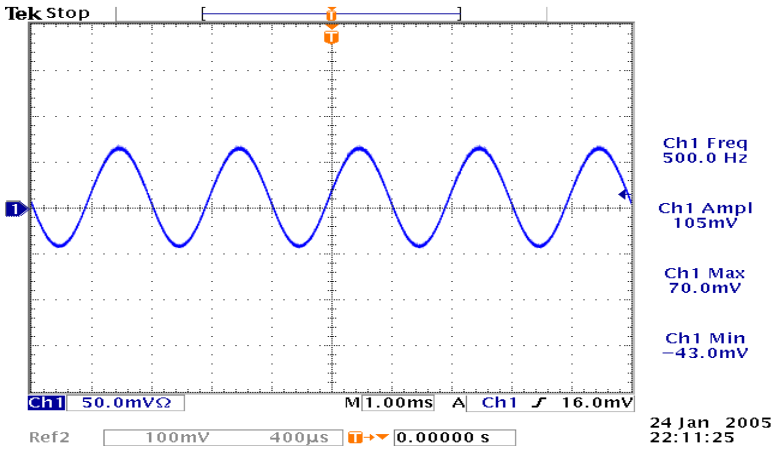

Fig.3. 6 Waveform of induced current without diode in the rotor coil

From the experimental results, it can be seen that when AC voltage is applied to one set of exciting stator coil, AC current will be induced in the rotor coil if there isn't rectifier diode in the rotor winding. However, DC current will be induced in the rotor coil due to the existence of rectifier circuit, and the induced current has the same frequency as the exciting current. This further verified that the magnetized rotor could work just like a permanent magnet.

Fig.3.7 gives the results of both exciting current and induced rotor current.

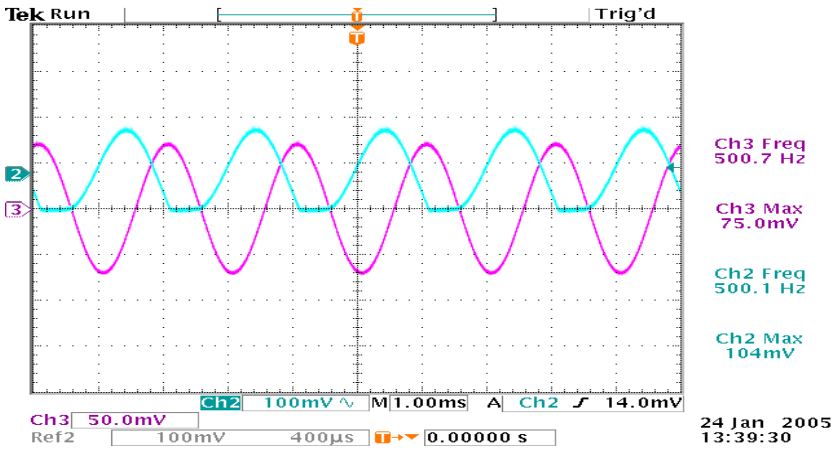

Fig.3. 7 Exiting current and induced rotor current

3.2.2 Variable relationships

Induced current versus frequency

With the test instrument as shown in Fig.3.3, the relationships between all kinds of variables have been investigated. The results are shown in the following figures.

The measured induced current with and without diode in the rotor coils are given in Fig.3.8 and Fig.3.9, respectively

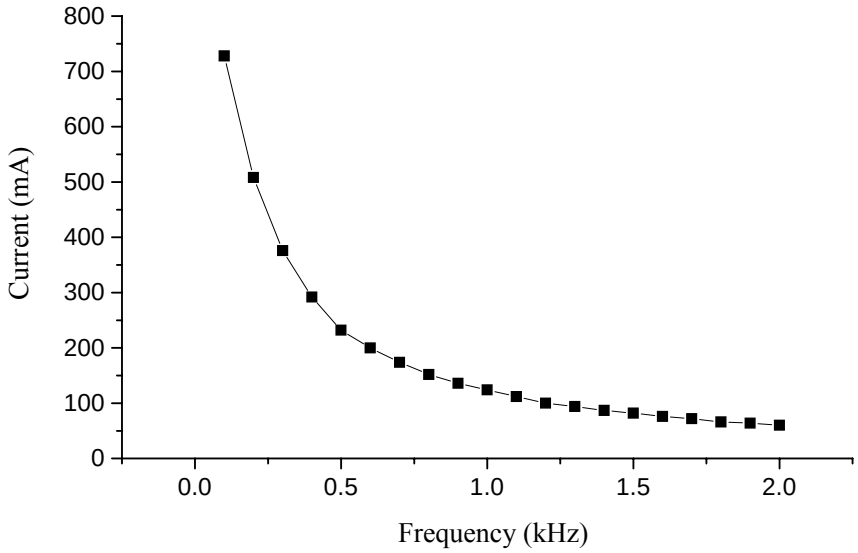

Fig.3. 8 The induced current without rectifier in the rotor coil

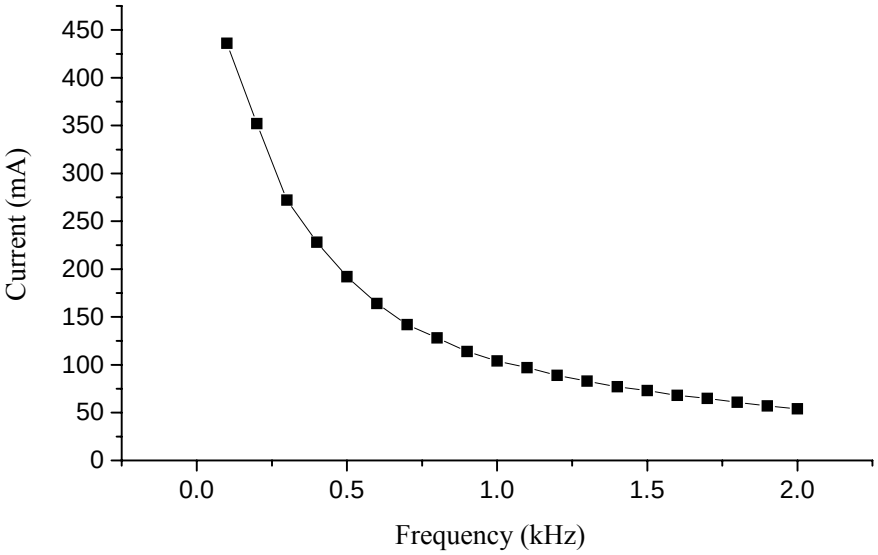

Fig.3. 9 The induced current with rectifier in the rotor coil

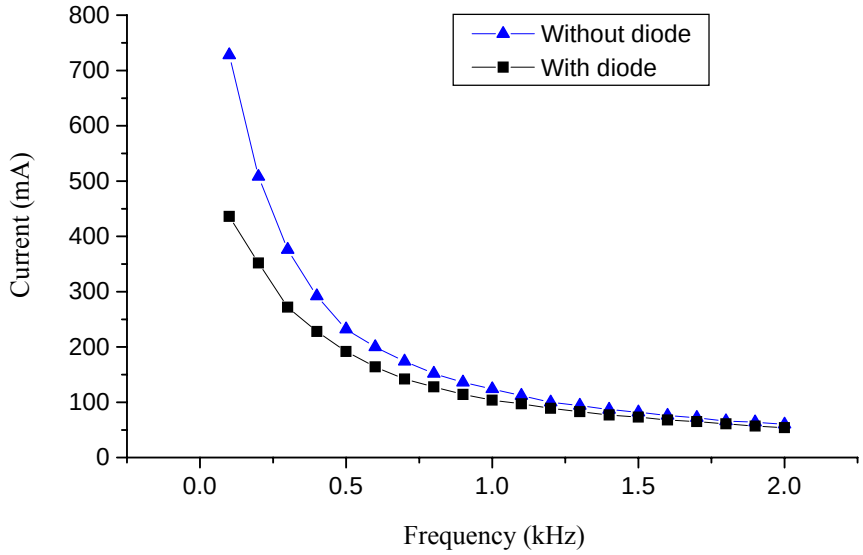

Fig.3. 10 The comparison of induced current with and without diode

From these figures, it can be seen that the induced current will decrease with the increasing of the exciting voltage frequency. A relatively large current can be induced in the low frequency range.

As can be seen in Fig.3.10, at the low frequency zone, the amplitudes of induced

rotor currents are very different with and without diode in the rotor circuits. The reason is that when there is a rectifier in the rotor coils, the negative part of the waveform is clipped out, so the amplitude of the induced current decreased with diode in the rotor circuits.

Induced current versus air gap

The instrument shown in Fig.3.11 is used to measure the induced current and radial force versus air gap. When there is a diode in the rotor coils, the induced rotor current is measured with changing of the air gap, and the result is shown in Fig.3.12.

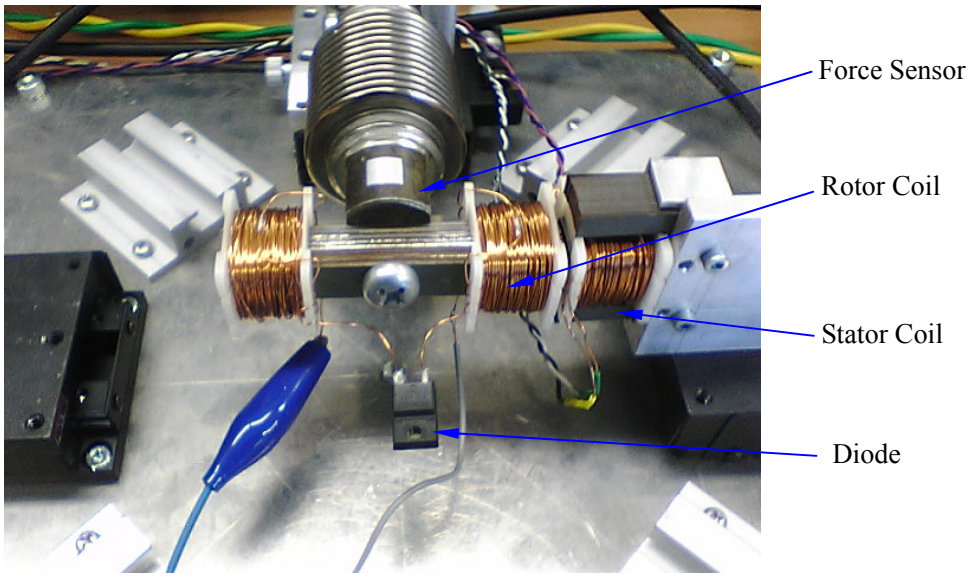

Fig.3. 11 Test instrument of rotor with rectifier circuit

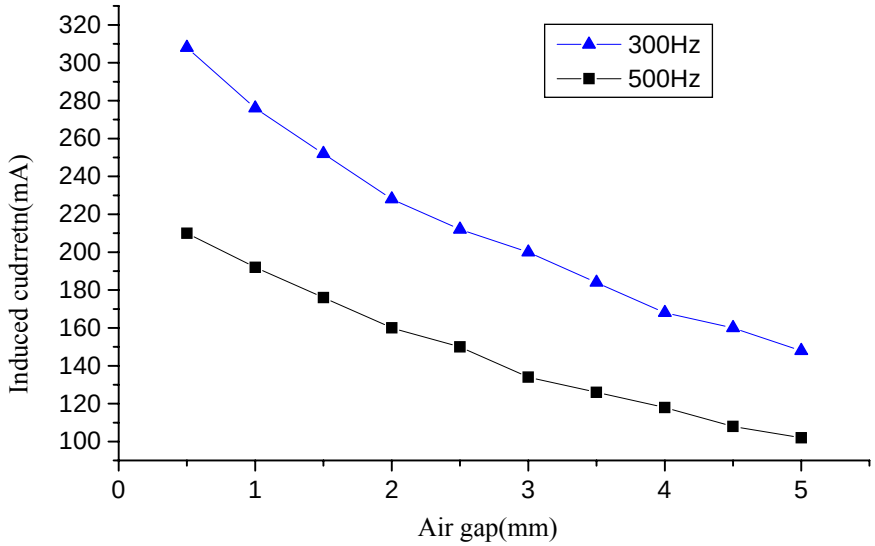

Fig.3. 12 The induced rotor currents versus air gaps

Fig.3.12 presents that the induced current has an inverse proportional relationship with the air gap. The magnitude of the induced current will decrease with the increasing of the exciting voltage frequency.

Flux density with respect to air gap

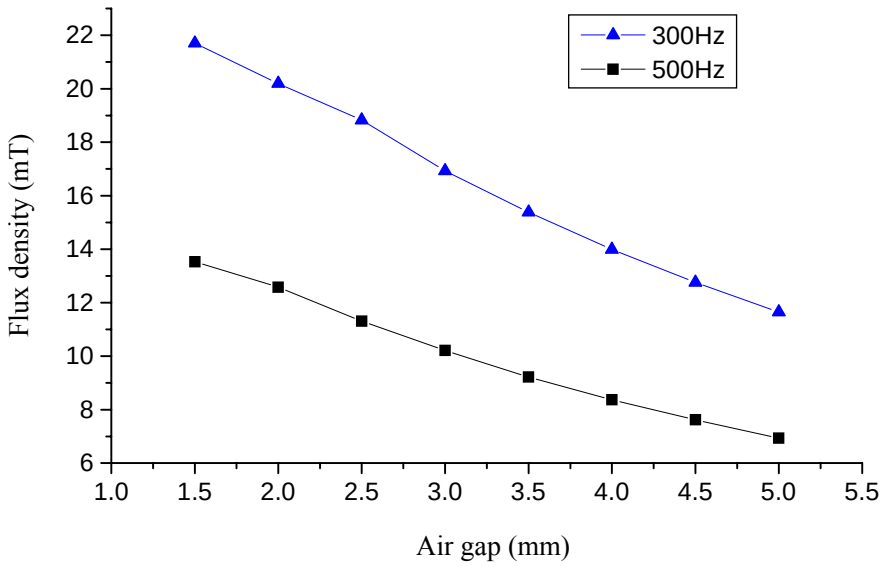

Fig.3. 13 Flux density versus air gap

From Fig.3.13, it can be seen that the flux density has an inverse proportional relationship with the air gap. Low exciting frequency generates larger flux density.

Flux density with respect to exciting current

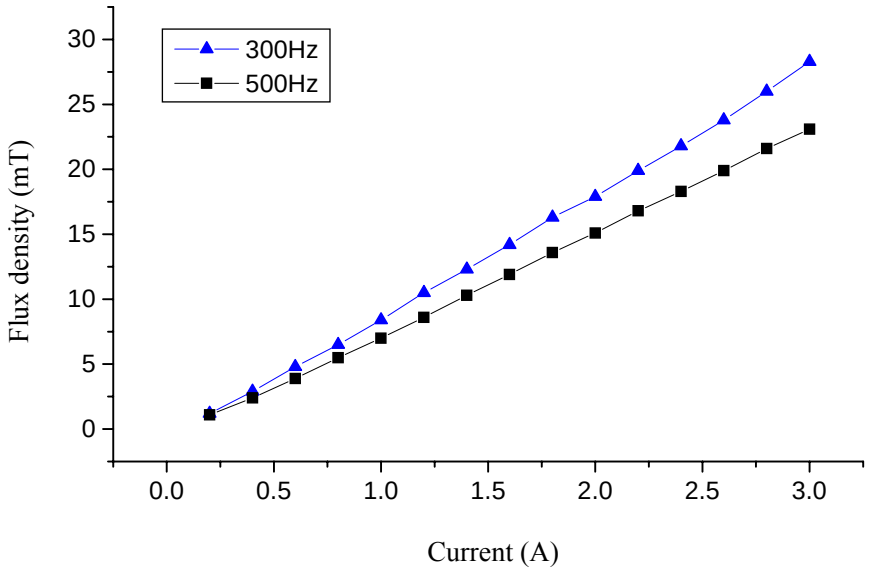

Fig.3. 14 The flux density with respect to exciting current

The flux density in the air gap with respect to exciting current at different exiting voltage frequencies is given in Fig.3.14. From this figure, it can be seen that the flux density has a linear relationship with respect to exciting current when keeping the air gap constant.

Flux density versus induced rotor current

The air gap flux density with respect to the induced current is shown in Fig.3.15. It can be seen that the flux density in the air gap has a linear relationship with the induced rotor current. And the flux density will increase with the induced current.

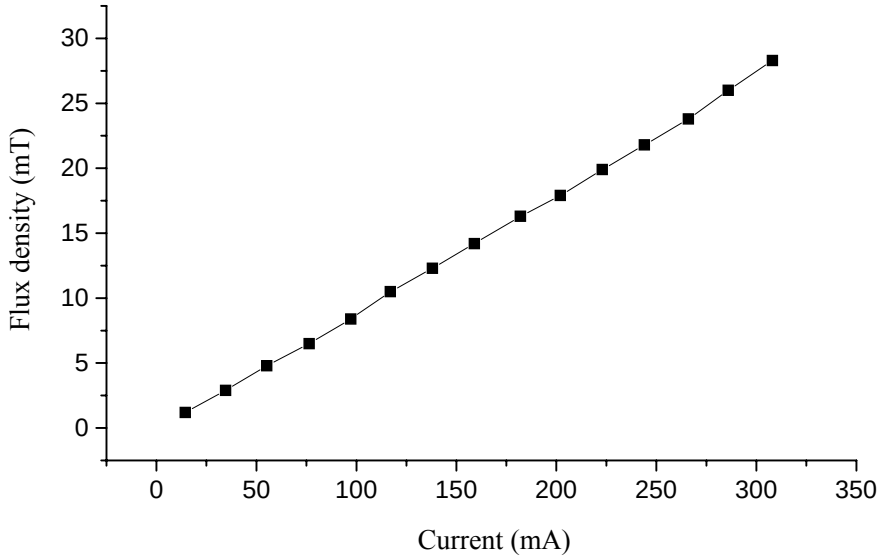

Fig.3. 15 Flux density versus induced rotor current

Flux density with respect to exciting current frequency

Fig.3.16 presents that if the magnitude of exciting voltage is constant, the magnitude of the flux density will decrease with the increasing of exciting current frequency, and there is a nonlinear relationship between the flux density and the exciting current frequency, and it also suggests that a relatively greater flux density can be obtained under the lower frequency zone.

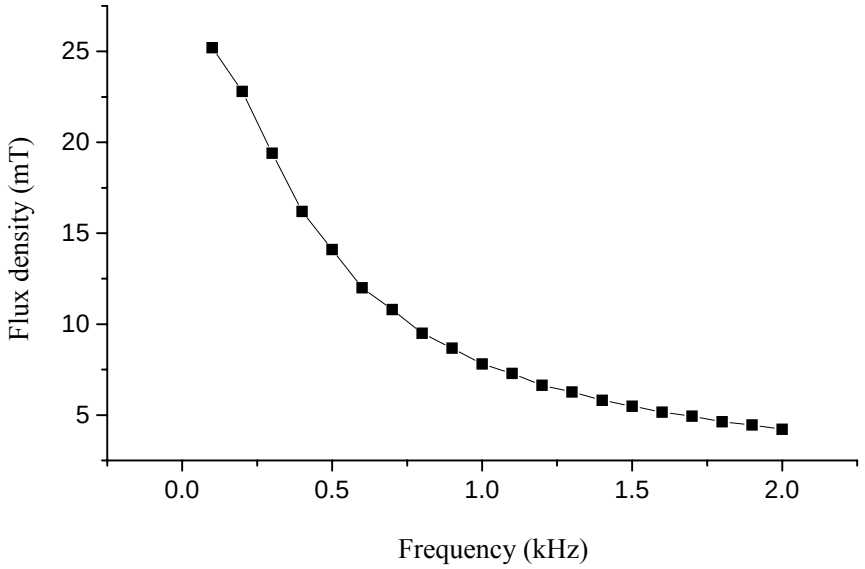

Fig.3. 16 Flux density with respect to exciting current frequency

Flux density against control current

When the amplitude of the AC exciting current V=14V, and the air gap g=1.5mm, the measured results of flux density changing with the control current are shown in Fig.3.17.

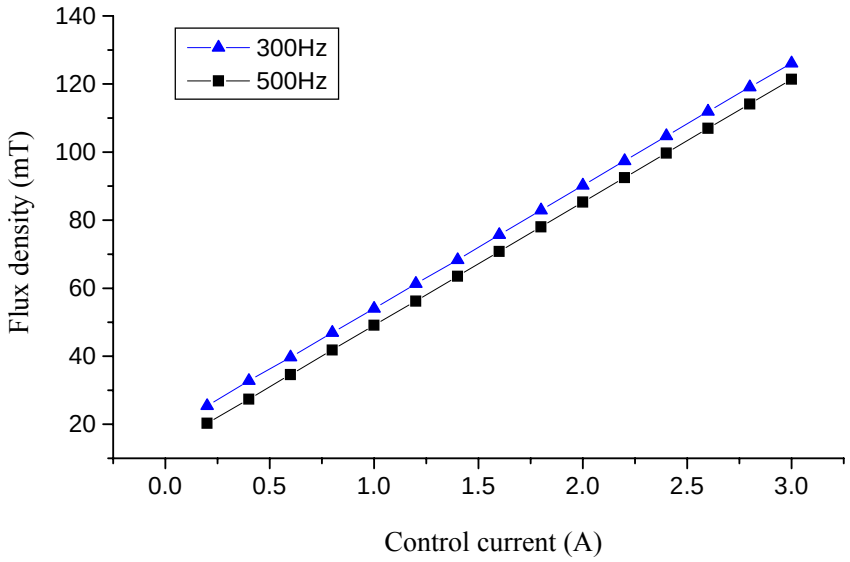

Fig.3. 17 Flux density with respect to control current

It can be seen that there is linear relationship between the flux density and the control current, and this figure also indicates that a larger flux density can be obtained at the lower exciting current frequency.

Induced current in rotor coil with respect to exciting current

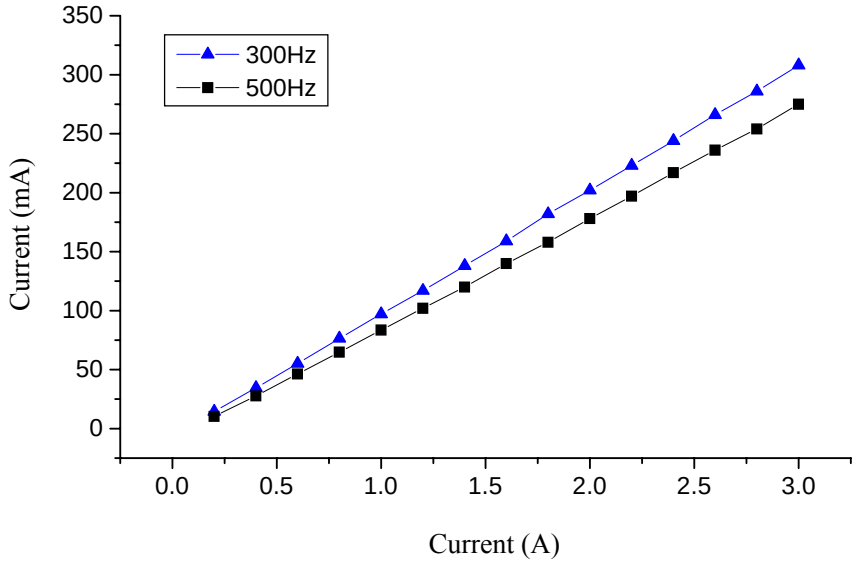

Fig.3. 18 Induced current with respect to the exciting current

It can be seen that in Fig.3.18, the induced rotor current has a linear relationship with the exiting currents, and a relatively larger induced current can be obtained at lower frequency. Furthermore, the magnitude of the induced current will increase with the exciting current.

Radial force versus air gap

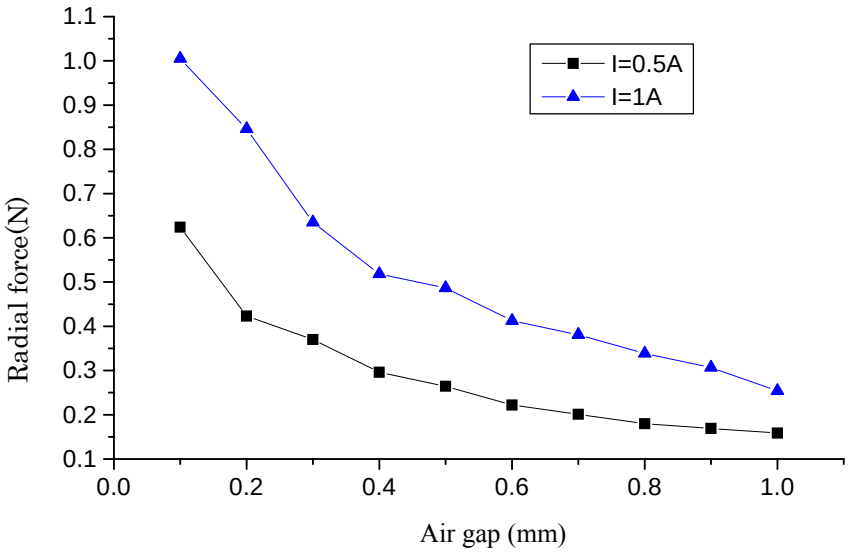

Fig.3. 19 Radial force versus air gap

From Fig.3.19, it can be concluded that the relationship between the radial force and the air gap and control current

$$F = k\frac{i_c^{\,2}}{g^2} \tag{3.8}$$

where F is the radial force; g is the air gap; i_c is the control current; and k is a coefficient.

Radial force versus control current

The results shown in Fig.3.20 further verify formula (3.8). The radial force will increase with the control current. A relatively large radial force can be obtained at the lower exciting frequency.

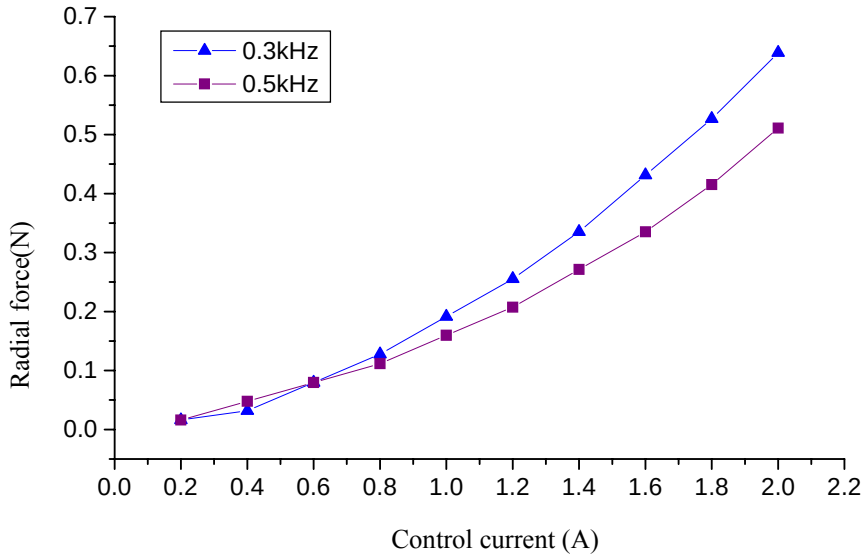

Fig.3. 20 Radial force with respect to the control current

3.3 Summary and Remarks

The feasibility analyses of the proposed bearingless motor with rectifier rotor coil are verified by numerical simulation preliminary. A simple test instrument in 1 DOF has been built, and the relationships between all of the variants have been measured. These results will provide an instructive direction for the following design work.

Chapter 4 FEM and Experimental Study Using Prototype I

4.1 Configuration of Prototype I

Based on the analyses and experimental results in the former chapter, a test machine of bearingless motor with rectifier rotor coil is built. The configuration is shown in Fig.4.1. The air gap is 0.5mm, the outer diameter of the stator is 70mm, and the outer diameter of rotor is 33mm (see Table 1). With this test machine, a series of experiments have been carried out to investigate the performance of the proposed rectified bearingless motor.

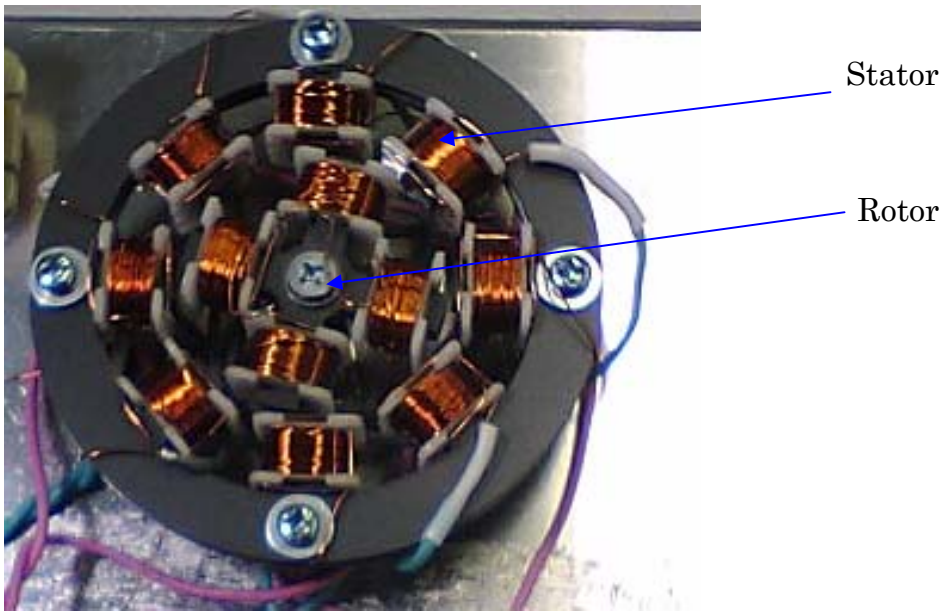

Fig.4. 1 Configuration of prototype bearingless motor with rectifier rotor

Table 1 Dimensions of prototype I

Average air gap	0.5mm
Stator outer diameter	70mm
Inner diameter of stator	54mm
Rotor outer diameter	33mm

4.2 Basic Relations Between Different Variables

4.2.1 Radial forces versus control current

First, the problem how many turns of rotor and stator coils can generate the optimal radial force has been studied by experiment.

When the control coil is 100 turns, exciting coil is 56, rotor is 500×2 turns, exciting voltage is 0Vp-p, 10Vp-p and 20Vp-p respectively, *f*=500Hz, air gap=1mm, the radial force versus the control current is given in Fig.4.2. (Only left-hand stator is applied the control current)

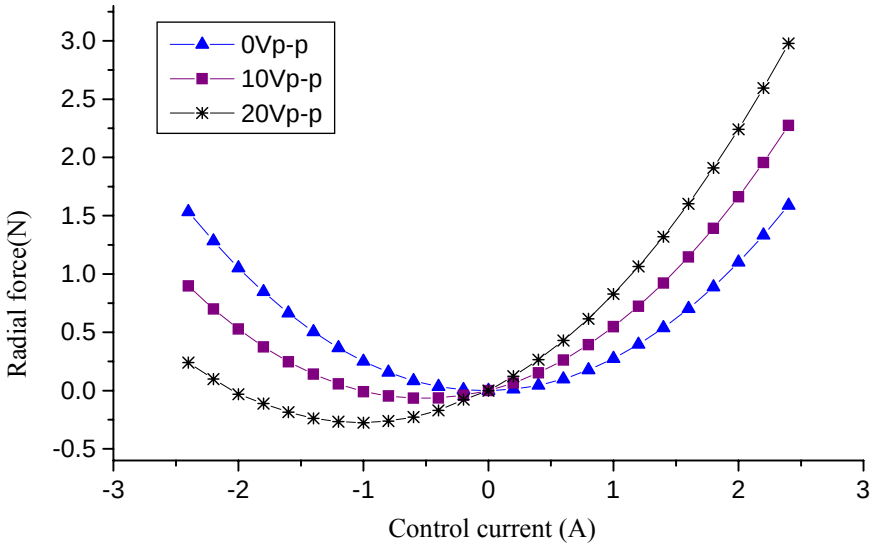

Fig.4. 2 Radial force versus control current

From Fig.4.2, it can be seen that the changing of exciting voltage will affect the radial force greatly. If there is no exciting voltage applied, the radial force does not change its direction as the control current direction is changed. However, when the exciting voltage is applied, the direction of radial force depends on the control current. That is, the negative force will be generated. This result further verifies that the magnetized rotor possesses the performance of permanent magnet. And the larger the applied exciting voltage is, the larger the negative radial force can be produced.

When the control coil is 100 turns, exciting coil is 56, the rotor is 500×2 turns, exciting voltage is 0Vp-p, 10Vp-p and 20Vp-p respectively, *f*=500Hz, air gap=1mm, the radial force versus the control current is shown by Fig.4.3. (Only right-hand stator is applied the control current)

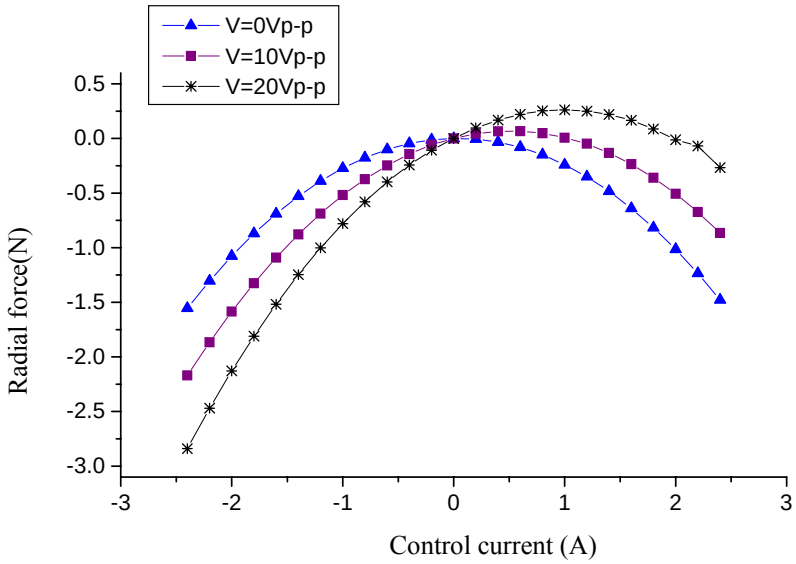

Fig.4. 3 Radial force versus control current

Fig.4.3 shows that symmetrical radial forces will be produced for the opposite control coils.

4.2.2 Radial forces versus the turn numbers of coil

When the exciting voltage is 20Vp-p, *f*=500Hz, the rotor is 500×2 turns, air gap is

constant, control coil is 56 turns, exciting coil is 100, 150, 200 turns respectively, the radial forces versus the control currents are shown in Fig.4.4.

It can be seen that when the same control current is applied to the control coil, the radial force increases with the decrease of turn numbers of exciting coil.

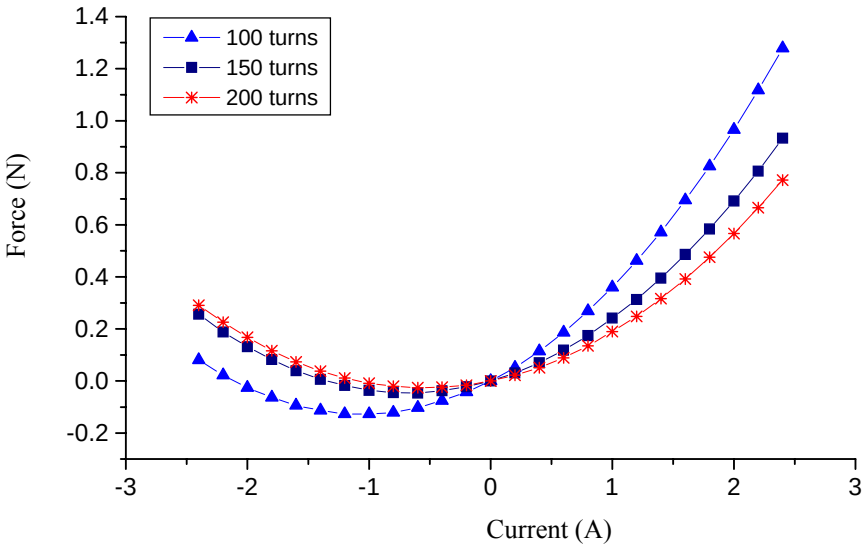

Fig.4. 4 Radial force versus control current

When the exciting voltage is 20Vp-p, f=500Hz, the rotor is 500×2 turns, air gap is constant, exciting coil is 56 turns, control coil is 50, 100, 150 turns respectively, the radial forces versus the control currents are shown in Fig.4.5.

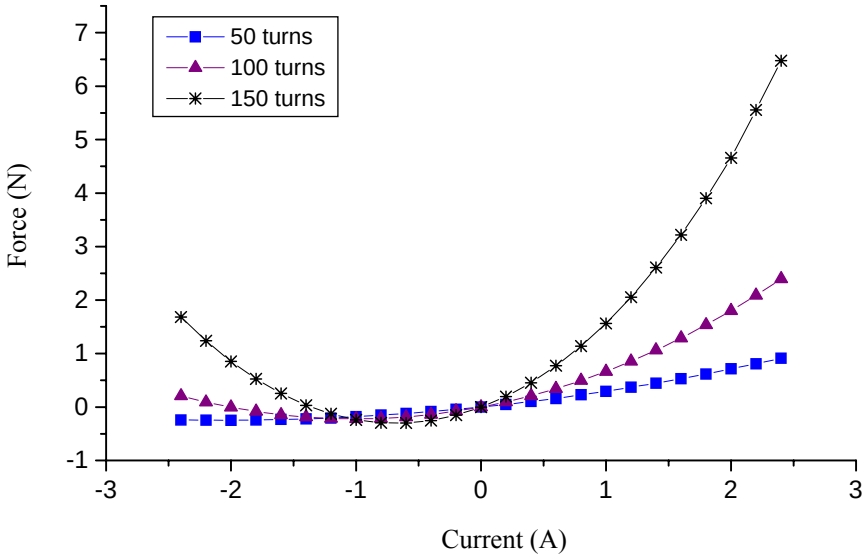

Fig.4. 5 Radial force versus control current

The figure shows that the turn numbers of control coil influence the radial forces greatly. If the turn number of control coil increases, the radial force increases correspondingly, furthermore, the radial force obtained will be increased greatly.

Comparison of different exciting winding turns

When the exciting winding is 14, 14×2 and 14×3 turns respectively, and control winding is 14×3 turns, rotor winding is 14×3×2turns, air gap is 0.5mm, exciting voltage is 6Vp-p, *f*=800Hz, the comparison of radial forces under different exciting winding turns is presented in Fig.4.6.

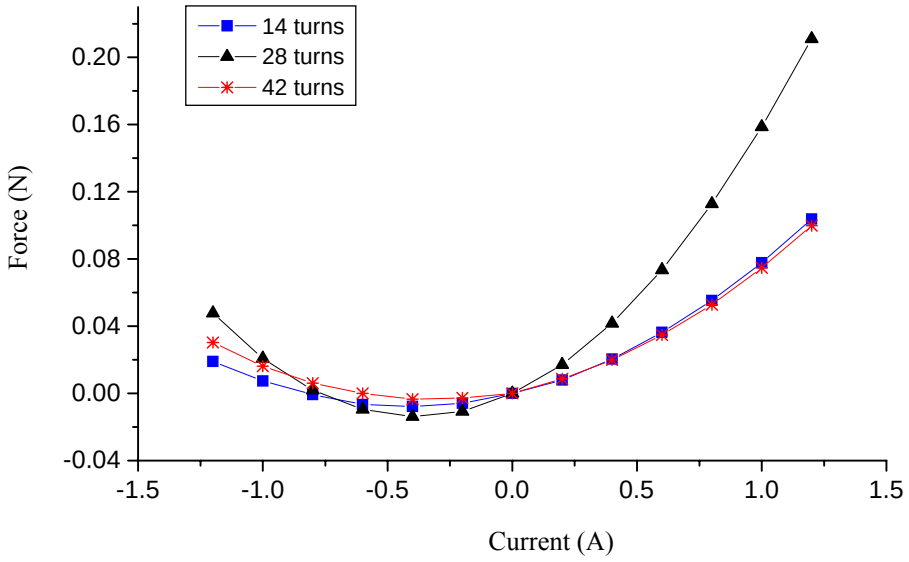

Fig.4. 6 Radial force versus control current

From Fig.4.6, it can be seen that when exciting winding is 14×2 turns, the waveform obtained is much better than the others.

4.3 Determination of Coil Turns and Studies on Prototype I

Comparing the results obtained in section 4.2, the turn numbers of exciting winding, control winding, and rotor winding are determined as 14×2 turns, 14×3 turns, 14×3 ×2turns respectively, and the air gap is 0.5mm. Based on these dimensions, the realization of levitation and rotation is investigated for the proposed rectified bearingless motor.

The comparison of force versus control current is given in Fig.4.7, as the exciting voltage is 6Vp-p and 0Vp-p, f=800Hz.

That is, while the air gap is kept to be 0.5 mm, the radial force is measured when regulating the control current. And the results are shown in Fig.4.7. It can be seen that the radial forces will not change their direction when the exciting voltage is 0 volts, and the blue curve shows the results when the exciting voltage is 6 volts. However, when the

exciting voltage is applied to the exciting coil, the negative force can be produced, which further verifies that the magnetized rotor has the characteristic of permanent magnet.

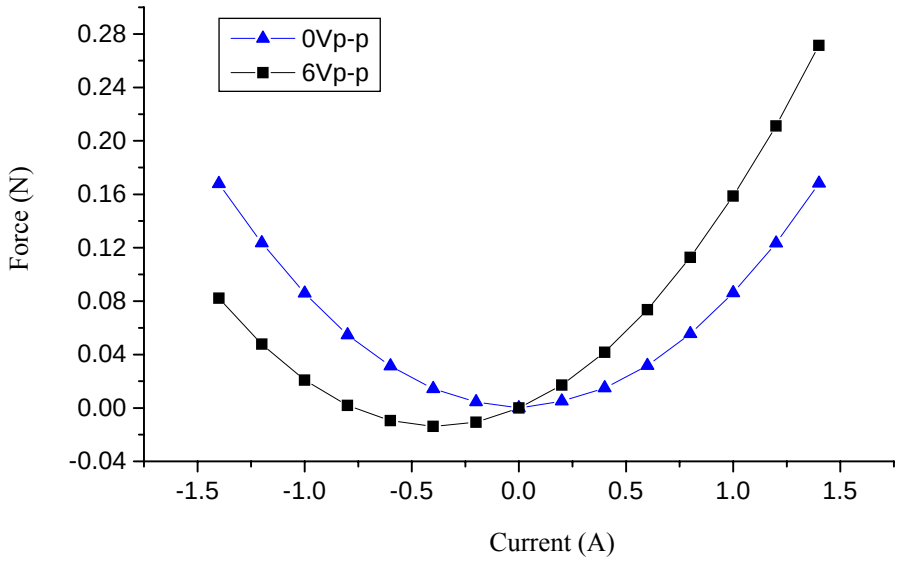

Fig.4. 7 Force versus control current

Fig.4.8 gives the results of flux density with respect to the control current. The air gap is kept to be 0.5mm, and the flux density is measured when regulating the control current.

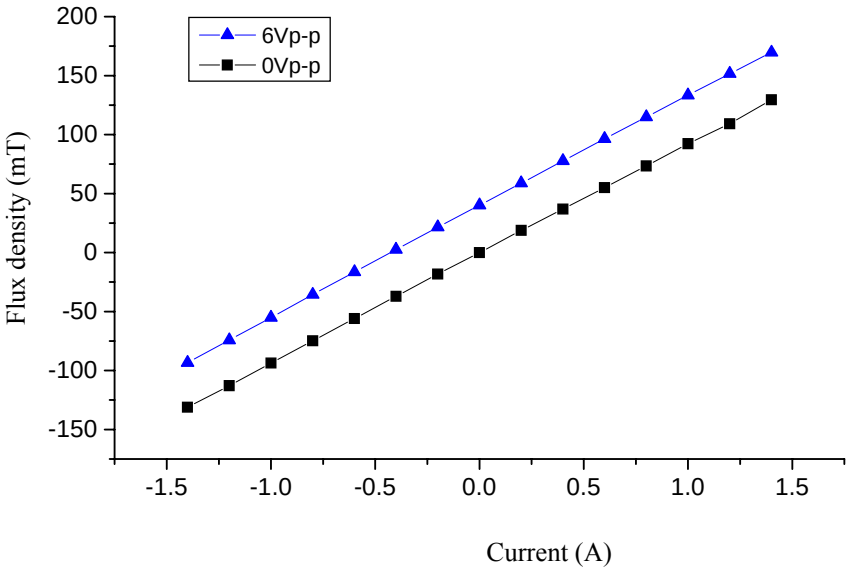

Fig.4. 8 Flux density versus control current

It can be seen that the line goes through the original point when the exciting voltage is 0 volts, nevertheless when the exciting voltage is 6 volts, there is a start value when the control current is zero. This figure also tells us that the magnetized rotor holds the performance of permanent magnet, the flux density in air gap increases with the the exciting voltage value, and they have a linear relationship.

Fig.4.9 shows that the leakage flux density has a linear relationship with the control current.

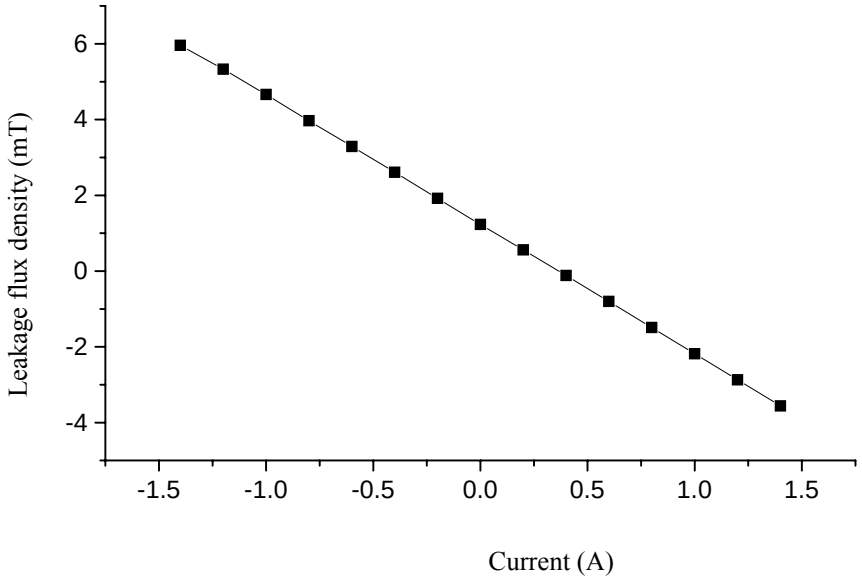

Fig.4. 9 Leakage versus the control current

4.3.1 Investigation of radial forces with FEM

Since it has been verified that the DC current will be induced in the rotor coil due to the existence of rectifier circuit, therefore, in the FEM analysis, we suppose that the rotors are magnetized by DC current. And the current will polarize the rotor poles just as shown in Fig.4.10. The control current arrangement is given in the same figure.

Current density : Istator=5.6/0.001**2, Irotor=5.6/0.001**2. With changing the rotor angular displacement, the radial forces are computed using the software ANSYS, and the flux distributions at different angular positions are shown in Fig.4.11.

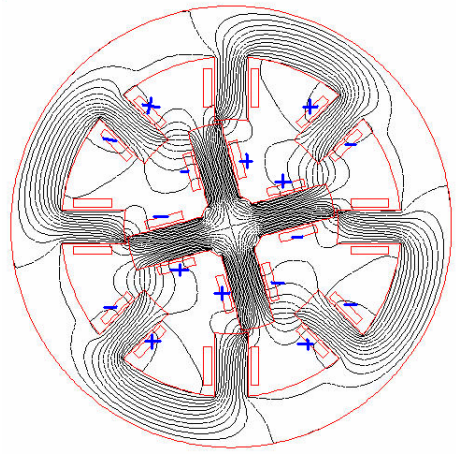

Fig.4. 10 Schematic of applied current

How the flux lines change with the rotor angular position are shown in Fig.4.11.

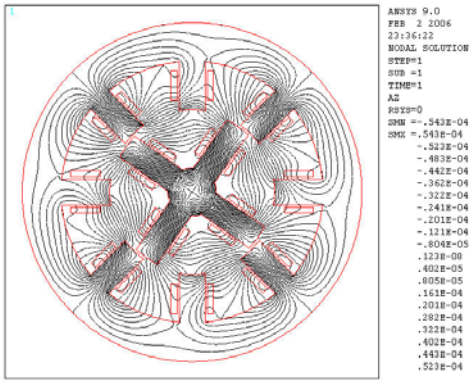

Rotor angular position -35°

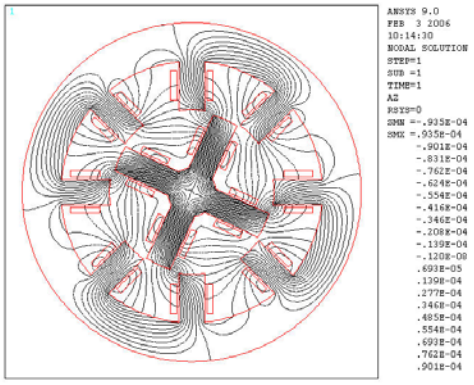

Rotor angular position -25°

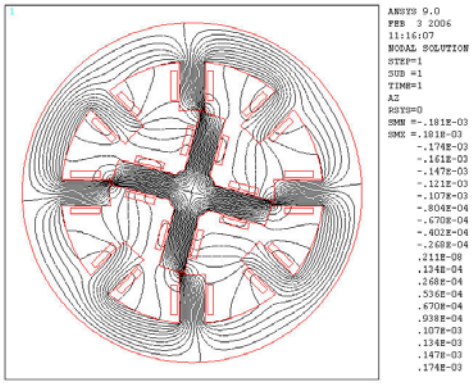

Rotor angular position -15°

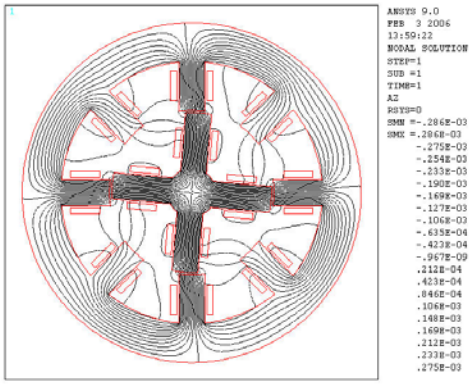

Rotor angular position -5°

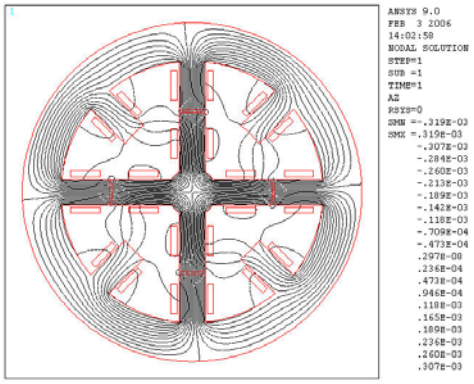

Rotor angular position 0°

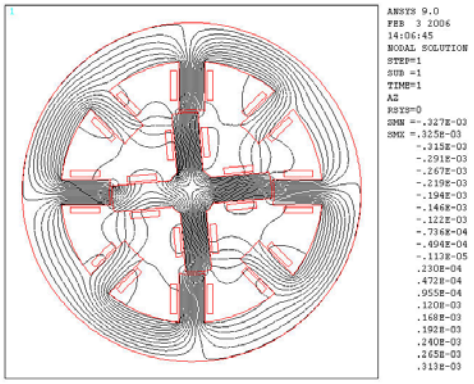

Rotor angular position 5°

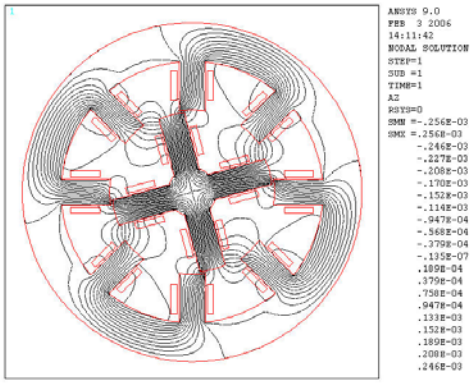

Rotor angular position 15°

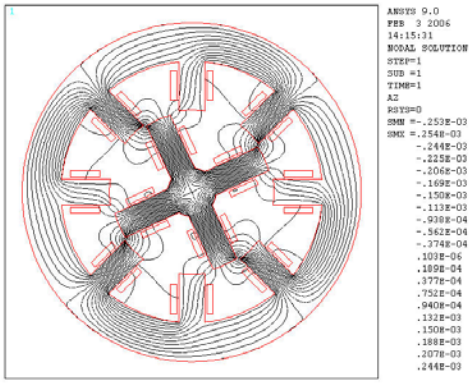

Rotor angular position 25°

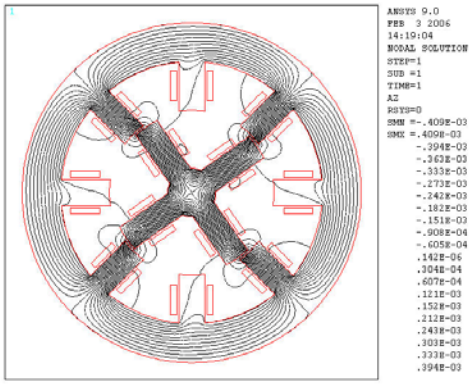

Rotor angular position 35°

Fig.4. 11 Flux distribution

Fig.4.12 and Fig.4.13 give the results of radial force versus the control current by

FEM and experiment respectively. It can be seen that these two results can verify with each other.

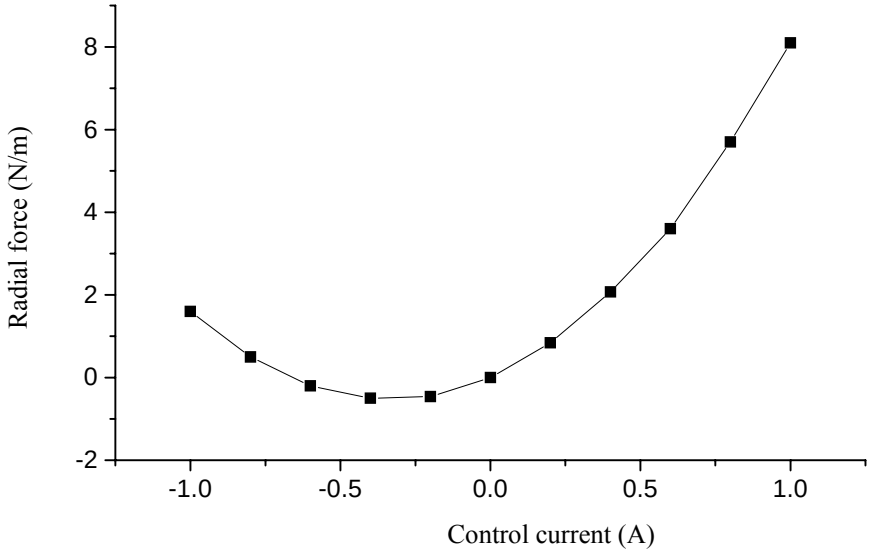

Fig.4. 12 Radial force versus control current (ANSYS)

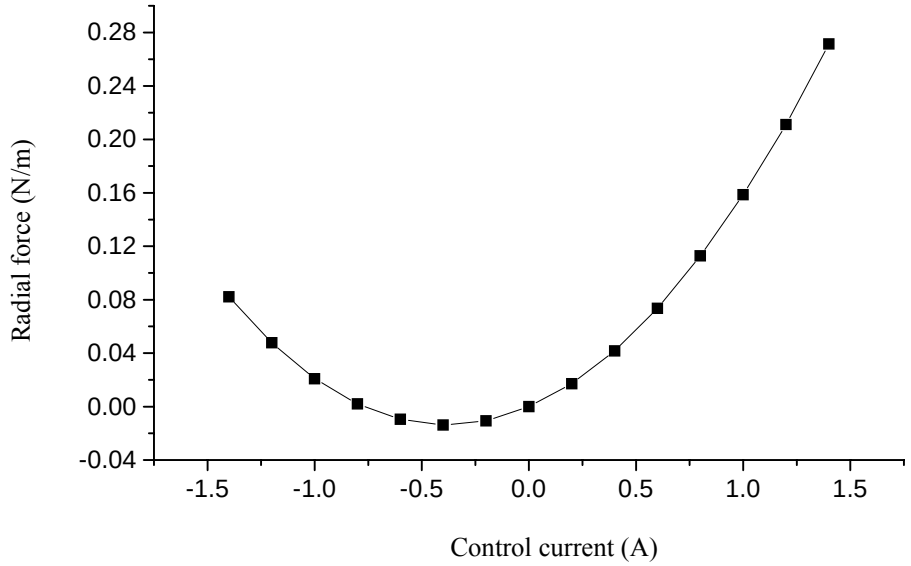

Fig.4. 13 Force versus control current (Experiment)

4.3.2 Experimental studies for rotation

Firstly, the rotor center is fixed using a mechanical bearing, we tried to rotate the rotor just like a permanent magnet stepping motor, but it is found that the rotor cannot be rotated as we supposed.

In order to find the reason, a series of FEM analyses and experiments have been carried out with the test model shown in Fig.4.1. The reason of the problem can be explained by the flux distribution shown in Fig.4.14.

As can be seen in these figures, only few of flux lines flow between the rotor and adjacent stator tooth, even with increasing the control current magnitude, there are still very few flux lines flowing through the adjacent rotor and stator. Therefore, it can be concluded that there exists zero torque position when the rotor and stator poles align with each other.

In order to solve this problem, the prototype II is designed.

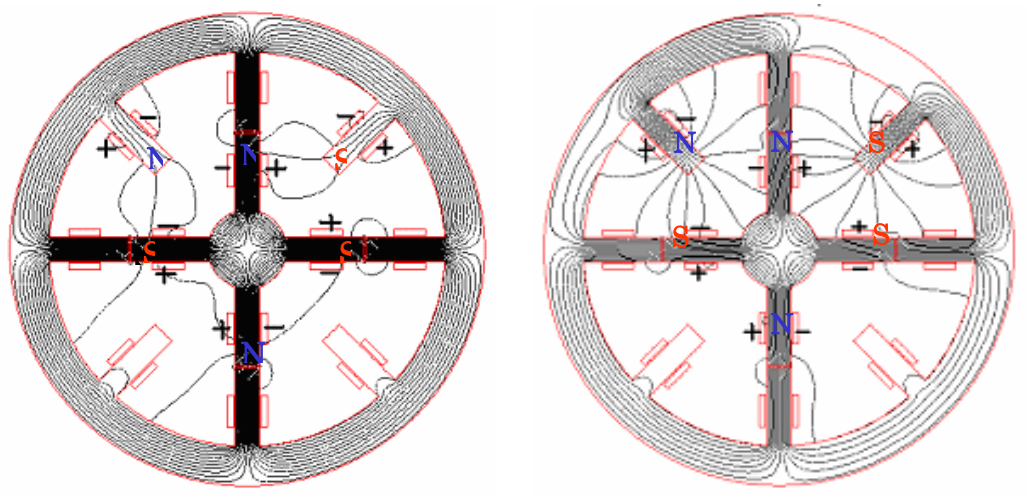

Control current density I_c=0.2A　　Control current density I_c=1A

Fig.4. 14 Flux distribution of prototype I

4.4 Summary and Remarks

With the prototype I, a series of studies are carried out. The variable relationships are investigated. However, for the practical experiment, the rotor cannot be rotated just as we supposed like a PM stepping motor. From the FEM analyses, the flux distribution shows that when the rotor poles align with the stator poles, there are only few flux lines flowing between the neighbored stator and rotor poles, therefore, the torque is not large enough to drive the rotor. Based on these analyses, the prototype test machine II is built.

Chapter 5 Design and Investigation of Prototype II

5.1 Design of Prototype II

5.1.1 Shape determination of prototype II

For the prototype I, the experiment results show that the radial force is not large enough to levitate the rotor, and there is a zero torque position when the rotor and stator poles align with each other, just like the position illustrated in Fig.5.1.

Since there is a large air gap between the adjacent rotor and stator, which causes a large reluctance between the adjacent rotor and stator teeth, and confines the flow of flux lines between them, therefore the values of radial force and torque will be small.

Maxwell force is the magnetic surface tension between the different medium boundaries, it is also called reluctance force. μ_{Fe} and μ_0 are the permeability of iron and air respectively; B_n and H_t are the normal direction magnetic flux density and tangential magnetic field intensity; since the magnetic flux lines entering or leaving the iron core are almost in a perpendicular direction, so $H_t \approx 0$. Then between the iron core and air gap interface, Maxwell force in unit area can be expressed as

$$\sigma = \frac{\mu_{Fe} - \mu_0}{2\mu_{Fe}\mu_0}(B_n{}^2 + \mu_{Fe}\mu_0 H_t{}^2) \approx \frac{B_n{}^2}{2\mu_0} \tag{5.1}$$

Then Maxwell force acting on the unit area dA of rotor outside surface is

$$dF_M = \frac{B_n{}^2 dA}{2\mu_0} \tag{5.2}$$

Thus the normal directional force F_n can be expressed as

$$F_n = \frac{B_n{}^2 dA}{2\mu_0} \tag{5.3}$$

From these formulas, it can be concluded that in order to increase the radial force and rotation torque, the overlapped area between the rotor and stator should be increased and furthermore, the air gap between the adjacent stator and rotor should be decreased. Based on these considerations, a new shape prototype test machine II is designed. The schematic of new shape rectifier bearingless motor is shown in Fig.5.1. The coils wound on the rotor and stator poles are as same as those shown in Fig.2.1.

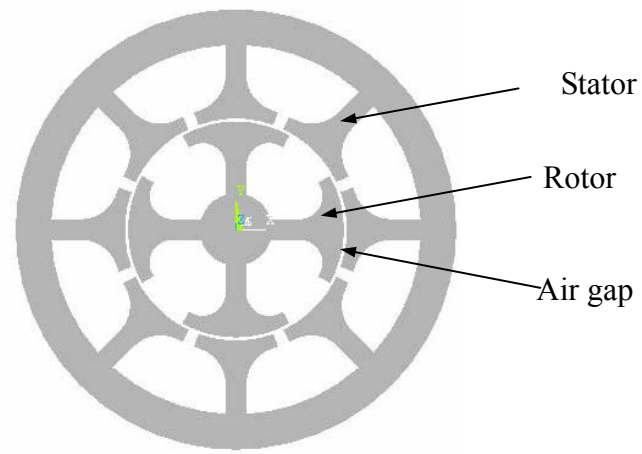

Fig.5. 1 The shape of protortype II

Table 2 Dimensions of prototype II

Average air gap	0.5mm
Outer diameter of stator	120mm
Inner diameter of stator	100mm
Outer diameter of rotor	59mm

The radius of the rotor is determined to be 60 mm. It is decided by easiness of treatment. The air gap is 0.5mm. As illustrated in Fig.5.1, the shape of the stator or the rotor is like an unfolded fan because of the necessity of increasing the section area where the stator and the rotor face to each other. The induced rotor current should be produced by mutual inductance, which depends on the faced area. The angle of the stator tooth is 40 degrees, which is twice to 20 degrees shown in Fig.4.2. This value is determined by the consideration for the widest stator tooth. The required angle for the gap to the next tooth is considered as at least 5 degrees. The angle of the rotor is indicated as α; the coils wound on the rotor and stator poles are identical to those shown in Fig.2.1.

5.1.2 The improvement design for prototype I

Since the shape of the rectified bearingless motor prototype II has been determined, an optimum dimension α of the bearingless motor is desired so that a relatively large radial force and torque can be generated. Based on the assumption that the rotor is located at the geometrical centre of the motor and it is magnetized by uniform induced DC current (the current density is 5.6/0.001**2), a series of FEM analyses have been carried out to determine the right value of α.

In order to obtain sufficient rotation torque to drive the rotor, the sine and cosine control current arrangement about the rotation angle is applied, as shown in Fig.5.2.

In the figure, θ is the rotational angle of the rotor, which rotates counterclockwise. The rotor position shown in Fig.5.2 corresponds to θ equal to 0 degree. The torques at various angular positions have been calculated when α changes from 15 degrees to 40 degrees with the incremental angle being 5 degrees. These variations of α are corresponding to the rotor tooth length being shorter, equal, and longer than the stator tooth length. Because of the symmetrical configuration of the rotor and the stator, analyses of the rotor angle θ change from 0 degree to 90 degrees have been examined. The results of torques are shown in Fig.5.3. As can be seen in the figure, when the angle of the rotor tooth increases, the curve of the torque becomes flat. But the magnitude will decrease. By comparison, it can be found that a relatively large and smooth torque can be obtained when α is equal to 30 degree. Thus, the 30 degrees of α has been

chosen for the prototype bearingless motor.

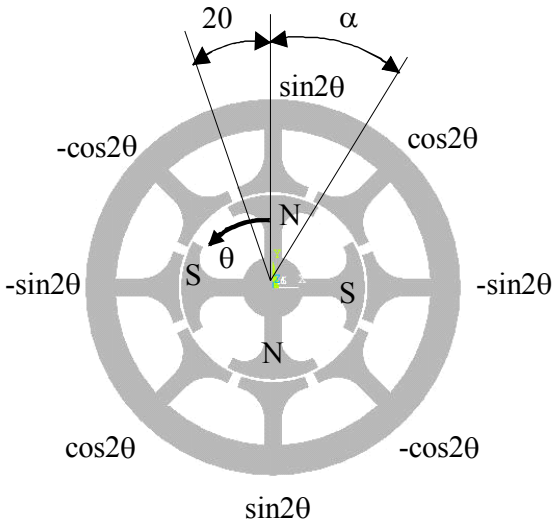

Fig.5. 2 Rotation strategy for the proposed bearingless motor

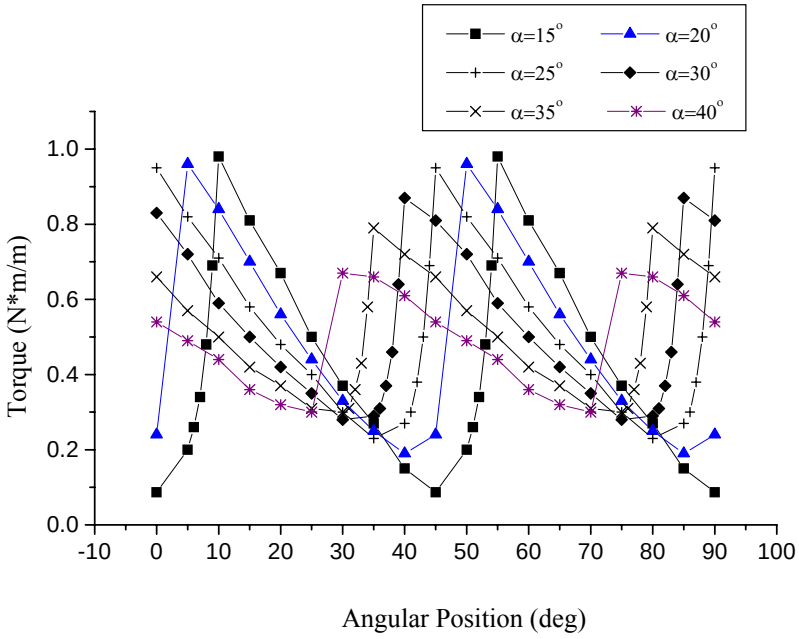

Fig.5. 3 Torques for different rotor dimensions

It can also be seen that the torque approaches its maximum when the rotor pole front

edge begins to overlap with the stator tooth face at all angles of α. Theses conclusions are given by the flux distribution shown in Fig.5.4. For example, when α is equal to 15 degree, and the rotor angle position α is 10 degrees, the torque reaches its maximum when the front edge of rotor pole begins to overlap with the next stator tooth face.

α=15, θ=10deg

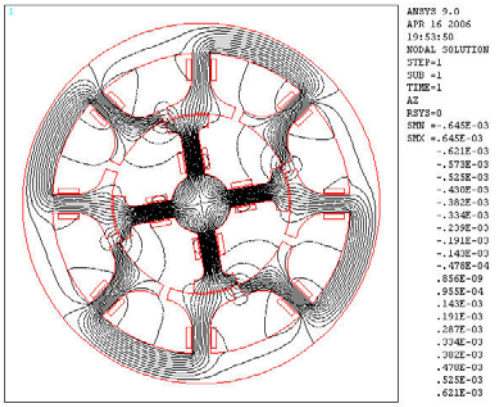

α=20, θ=5deg

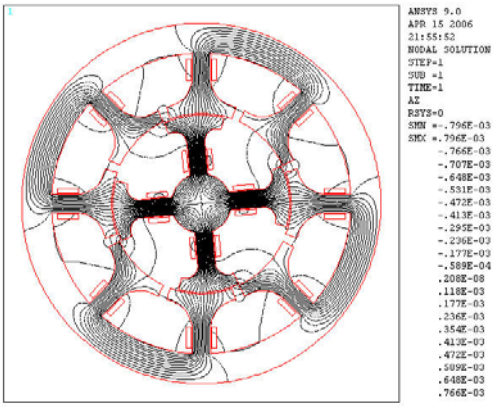

α=25, θ=0deg

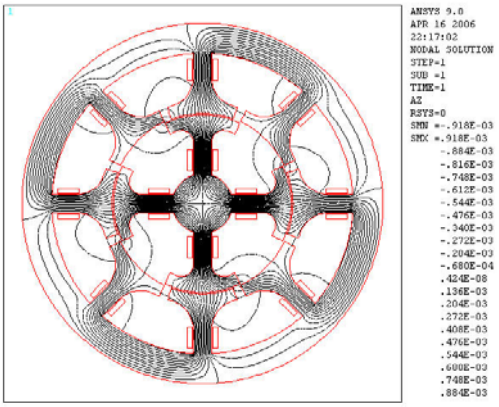

α=30, θ=40deg

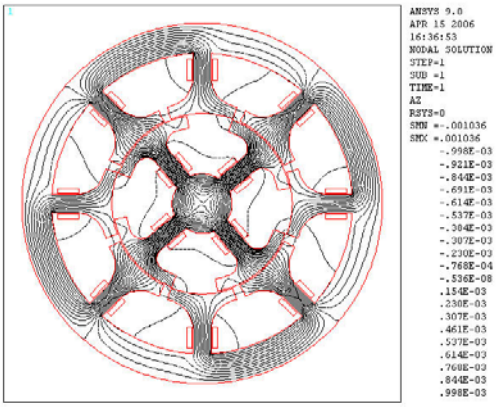

α=35, θ=35deg

α=40, θ=30deg

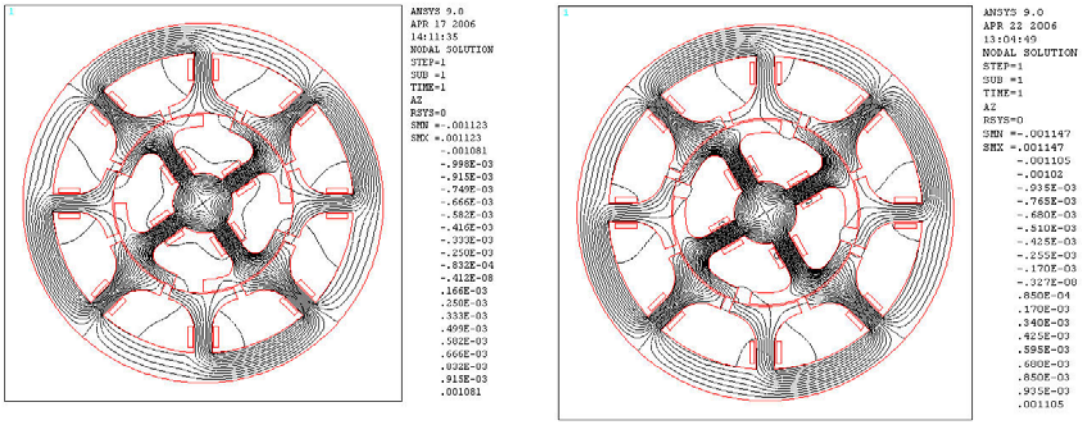

Fig.5. 4 Flux distribution at the maximum torque

From Fig.5.4, it can also be seen that the torque approaches its maximum when the rotor polar front edge begins to align with the stator tooth face at all α. For example, when α is equal to 15°, and the rotor angle position θ is 10°, the torque reaches its maximum, i.e. the rotor poles front edge begins to overlap with the next stator tooth face exactly.

Fig.5.5 shows the flux distribution at the minimum torque value.

α=15, θ=0deg

α=20, θ=40deg

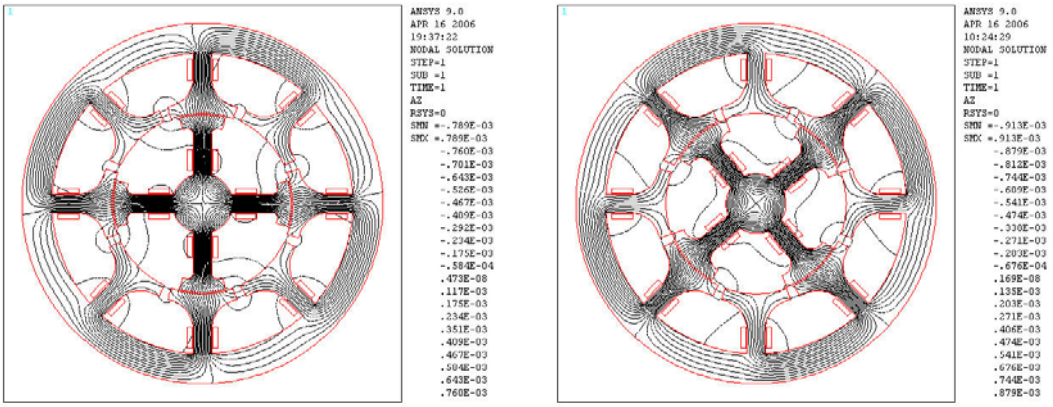

α=25, θ=35deg

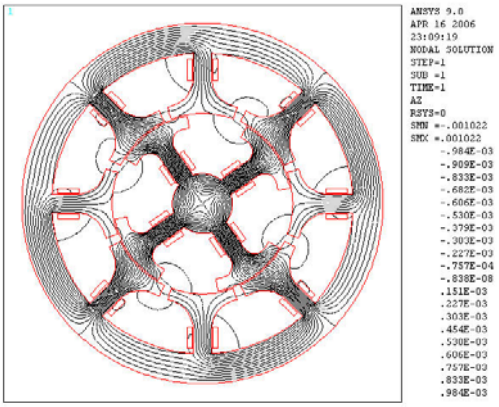

α=30, θ=30deg

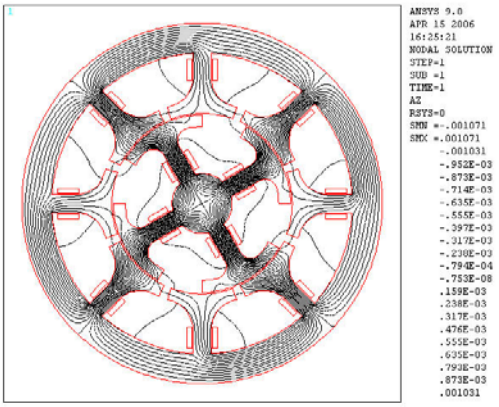

α=35, θ=30deg

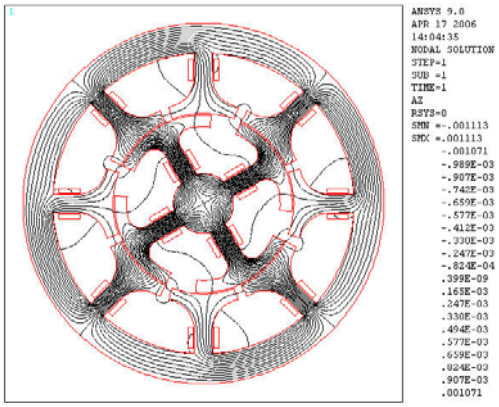

α=40, θ=25deg

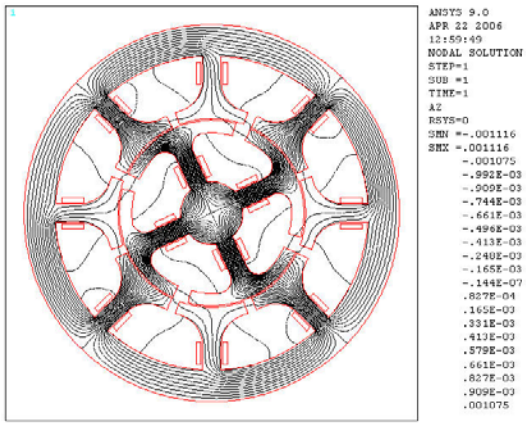

Fig.5. 5 Flux distribution at the minimum torque

5.2 FEM Analyses for Prototype II

5.2.1 Flux distribution of prototype II

Under the assumption that the rotor is located at the geometrical centre of the motor and it is magnetized by uniform induced current, and the rotation control current arrangement shown in Fig.5.2 is applied, α is equal to 30 degrees, the flux distributions when θ changes from 0 deg to 80 deg are shown in Fig.5.6.

θ equal to 10 degree

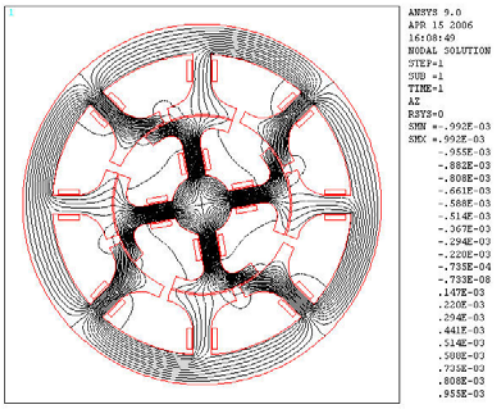

θ equal to 20 degree

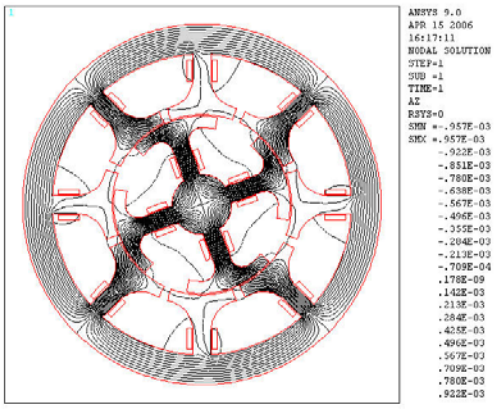

θ equal to 30 degrees

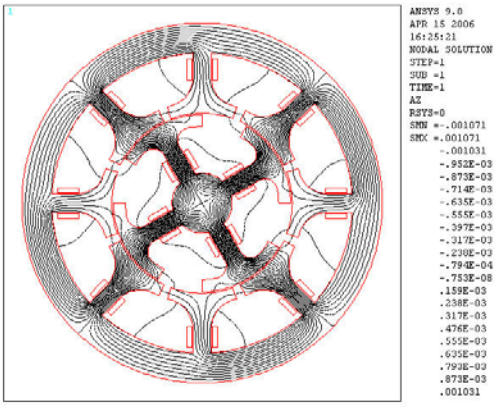

θ equal to 40 degrees

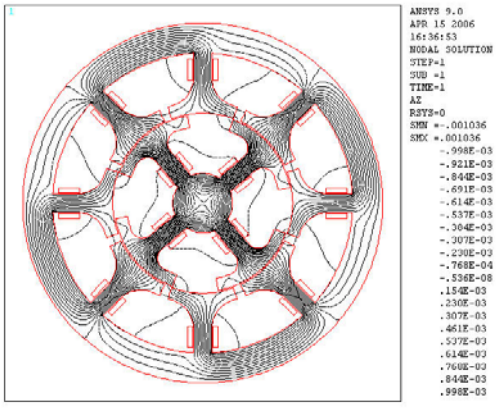

θ equal to 50 degrees

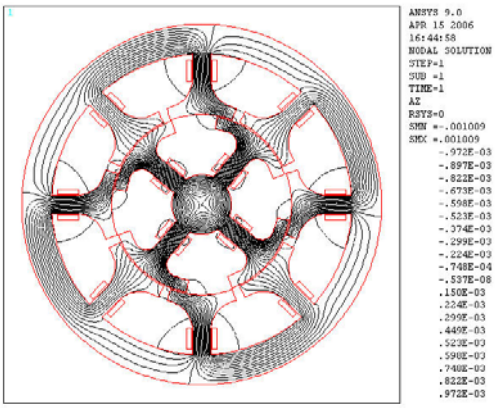

θ equal to 60 degrees

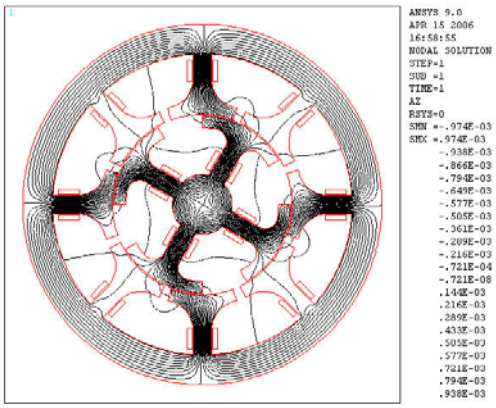

θ equal to 70 degrees

θ equal to 80 degrees

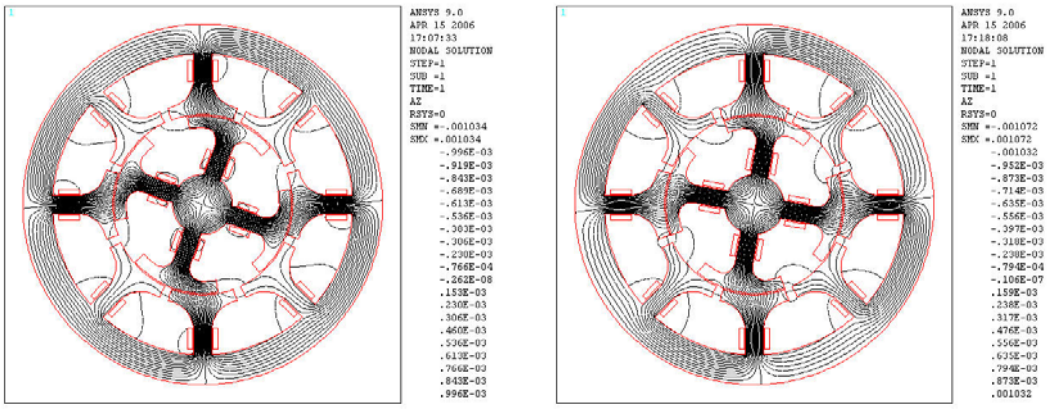

Fig.5. 6 Flux distribution with changing θ

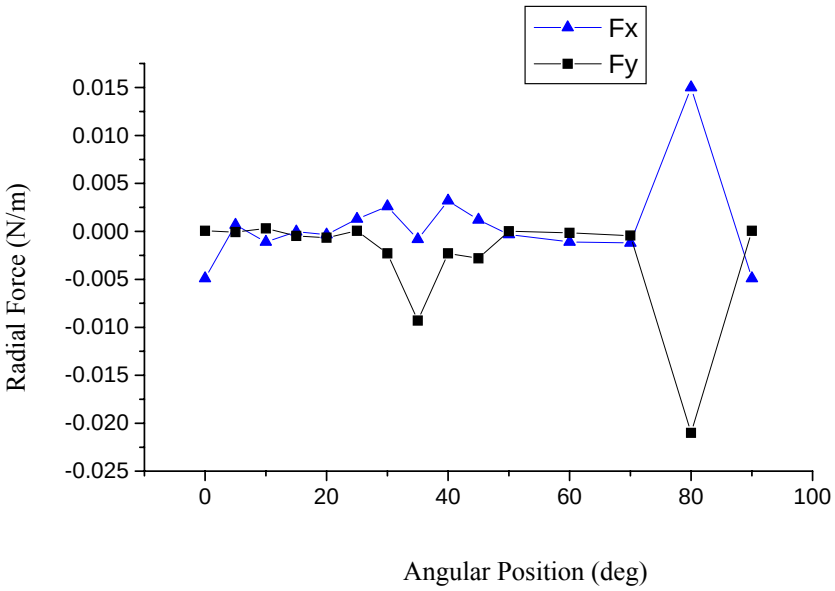

Fig.5. 7 Radial force corresponding to α equal to 30 degree

Fig.5.7 presents the result of radial forces versus the rotor angular positions. From this figure, it can be concluded that the radial force is very small and can be neglected, therefore this control current arrangement of rotor rotation will not interfere with the rotor radial force function, furthermore, there is a decoupling relationship between the

radial force and rotation torque.

5.2.2 The comparison between prototype I and prototype II

The performances of the prototype I and prototype II are compared when the same control currents shown in Fig.5.1 are applied to the two test machines. The flux distributions are shown in Fig.5.8. Compared with Fig.4.14, it can be seen that much more flux lines flow between the stator and the adjacent rotor tooth. And the flux distribution will change with the control current.

The comparison results about the radial force and rotation torque are shown in Fig.5.9 and Fig.5.10. It can be seen that much larger radial force and torque can be generated in the new test model, and there is no zero torque position in the prototype II.

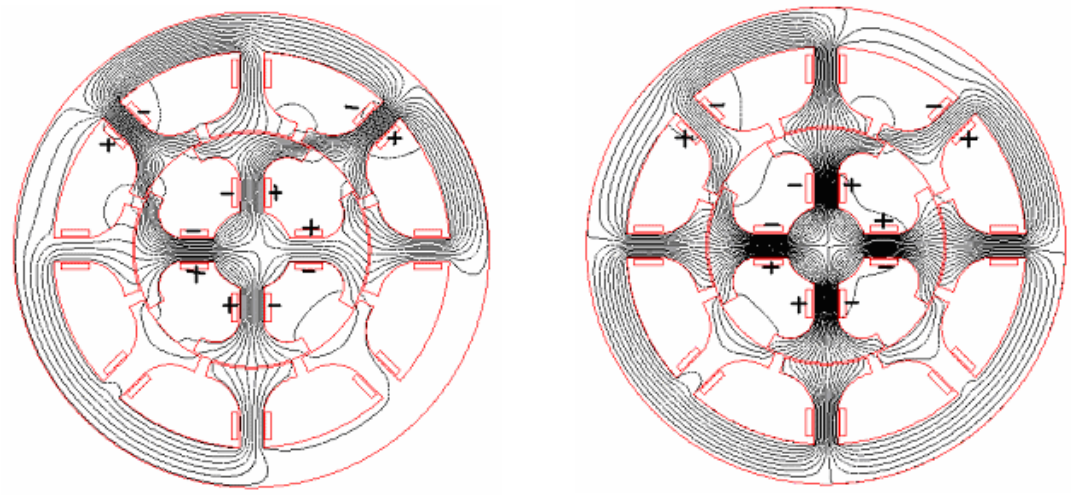

Control current density I_c=0.2A　　Control current density I_c=1A

Fig.5. 8　Flux distribution of α equal to 30 degrees

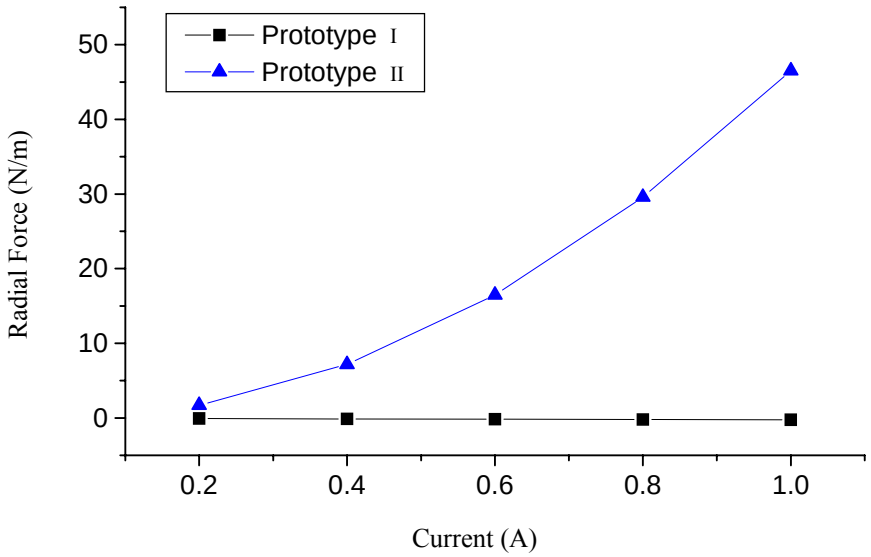

Fig.5. 9 Radial force comparison for the new and old model

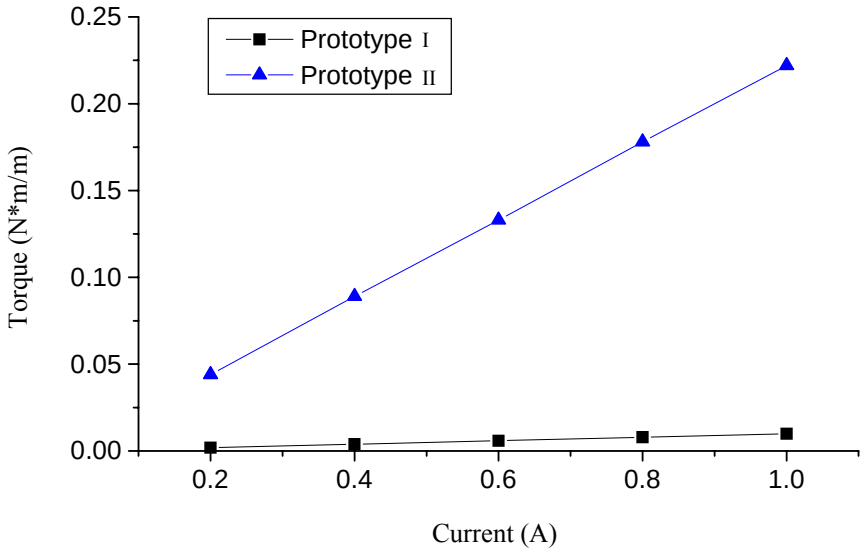

Fig.5. 10 Torque comparison for the new and old model

5.2.3 Decoupling relationship between the radial force and rotation torque

For bearingless motors, the major challenge lies in the design of a control device and algorithm that can control the radial forces without interfering with the function of the

motor. According to the assumption mentioned above, the radial forces and torques are adjusted by control current. In order to investigate the effect of control currents, based on the control current arrangement shown in Fig.5.2, a constant value β is superimposed upon the control current of the top stator pole and $-\beta$ is superimposed to the opposing stator pole, as illustrated in Fig.5.11. The torques have been calculated with the rotating of rotor, i.e. changing angle θ from 0 to 90 degrees. The constant value β is equal to 1, 3 and 5 respectively, and the results are given in Fig.5.12.

It can be seen that when the constant β is superimposed to the control current, the torque almost keeps no change, even if β is changed from 1 to 5. Therefore, it can be concluded that superimposing a constant to the control current will not interfere with the motor function, i.e. rotation torque. This conclusion gives us an instruction that DC current can be superimposed to the motor function to generate radial force, and there is no coupling between the motor and radial force function. This will contribute to the simplification of control strategy.

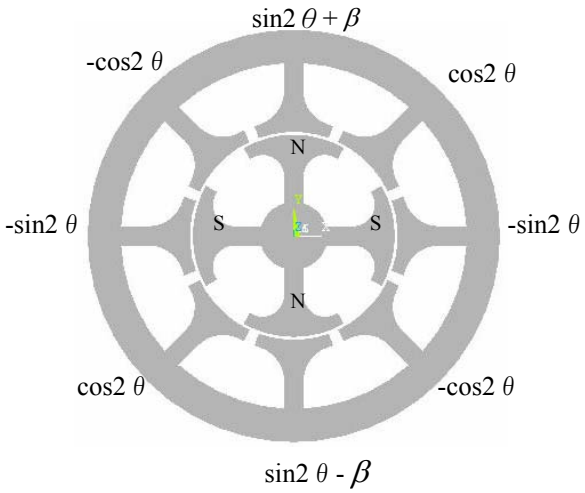

Fig.5. 11 Control current arrangement

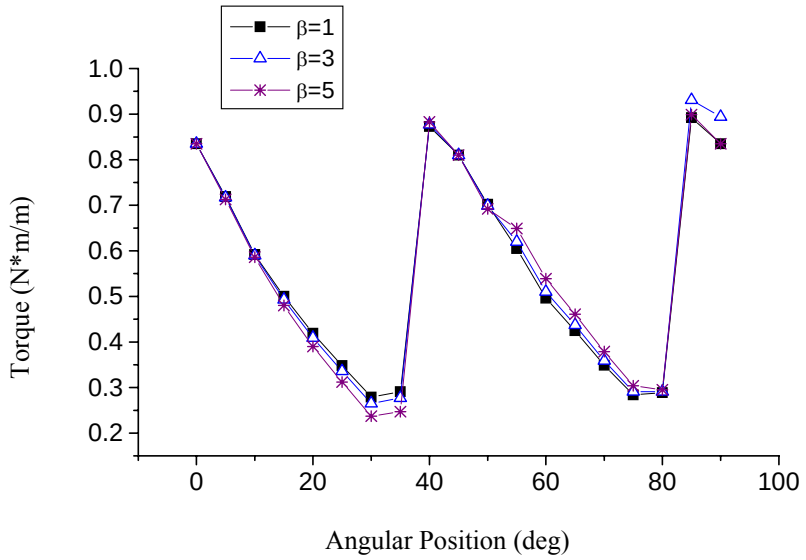

Fig.5. 12 Torques versus superimposed rotor angular position

5.2.4 Control current arrangement for radial force

In order to find the right control current arrangement for radial force generation, a series of computations have been carried out using FEM. Firstly, the vertical radial force has been considered. When the control current arrangement shown in Fig.5.13 is applied, the radial forces and torque have been calculated corresponding to various rotor angular positions. The results are shown in Fig.5.14 and Fig.5.15.

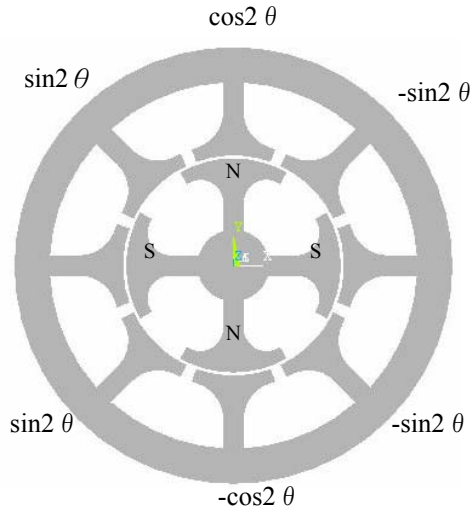

Fig.5. 13 Control current arrangement for radial force (*Fy*)

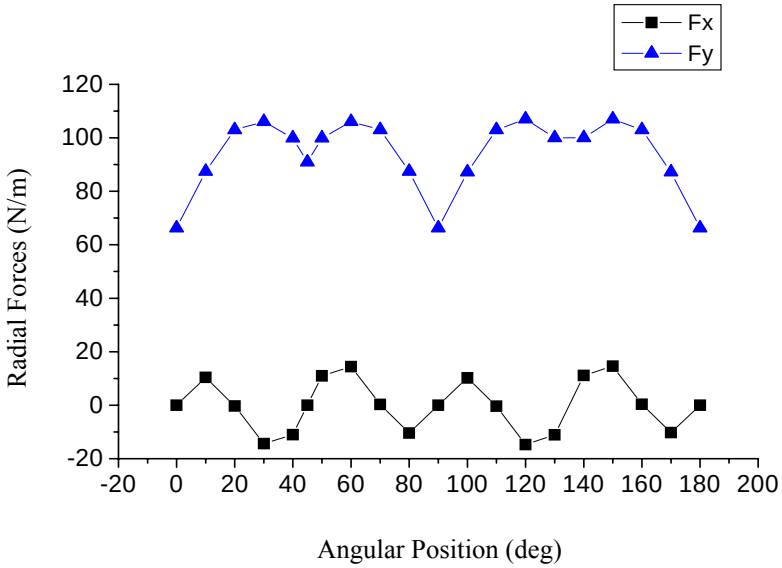

Fig.5. 14 Radial force versus rotor angular position

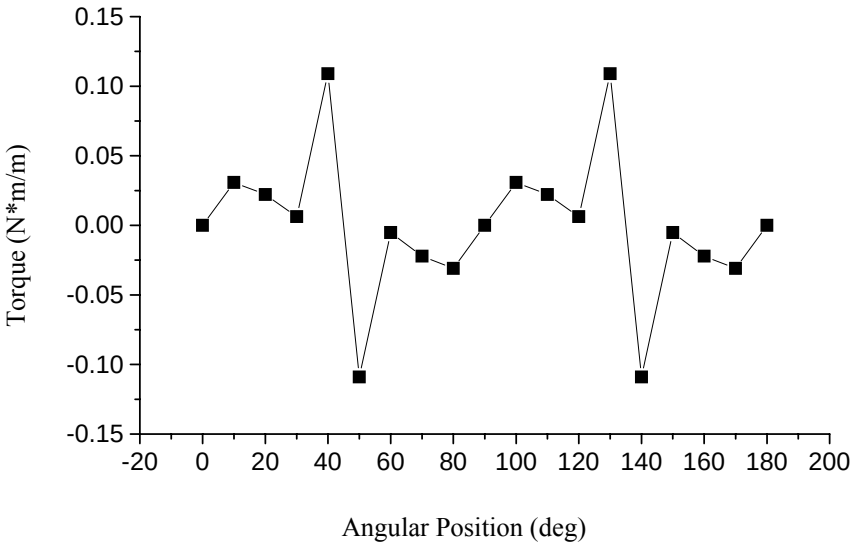

Fig.5. 15 Torque versus rotor angular position

When the radial force control current arrangement rotates 90 degrees in counterclockwise as shown in Fig.5.16, which are planned to be used to control the horizontal force, the radial forces and torque are also calculated corresponding to rotor angular positions, and the results are shown in Fig.5.17 and Fig.5.18.

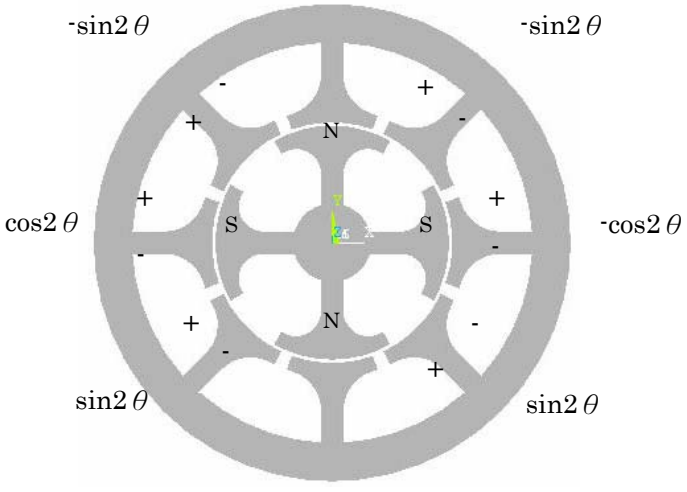

Fig.5. 16 Radial force control current arrangement (*Fx*)

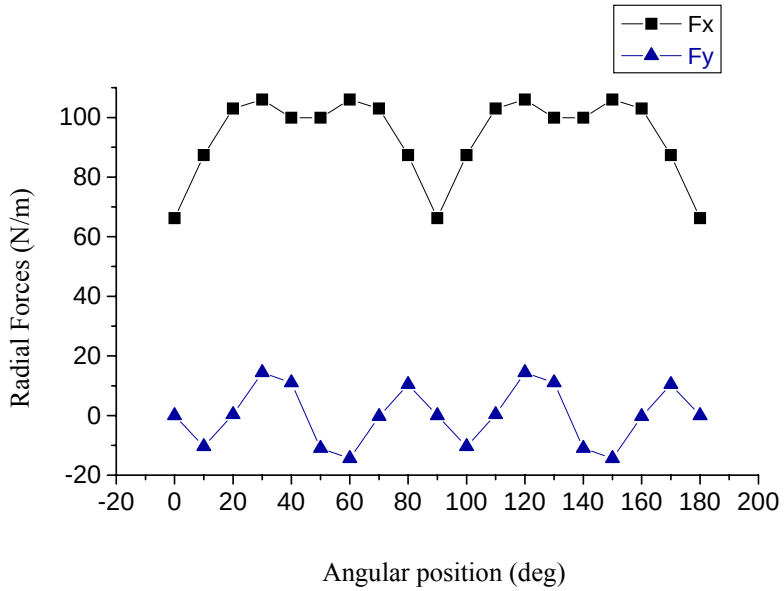

Fig.5. 17 Radial force versus rotor angular position

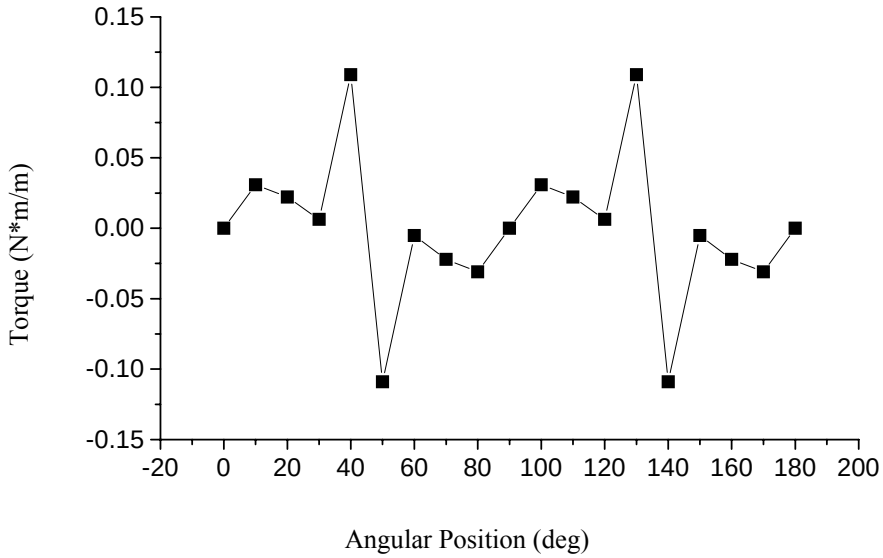

Fig.5. 18 Torque versus rotor angular position

From Fig.5.14 and Fig.5.17, it can be seen that the specified radial forces are about ten times to lateral forces. As a result, the radial forces can be guaranteed by the control current arrangements shown in Fig.5.13 and Fig.5.16. Fig.5.15 and Fig.5.18 give the torque values when the control current arrangements shown in Fig.5.13 and Fig.5.16 are applied. These values are very small, and they can be neglected in comparison with the toque values shown in Fig.5.3.

Therefore, the superimposition of the control current arrangements illustrated in Fig.5.2 and Fig.5.13 can be used to realize the rotor rotation and vertical radial force control, meanwhile the superimposition of the control current arrangements illustrated in Fig.5.2 and Fig.5.16 can be used to control the rotor rotation and horizontal radial force. In addition, these two functions will not interfere with each other.

For a bearingless motor, in order to keep the rotor balance, we hope to keep the radial levitation force constant when the rotor is rotating. However, as can be seen in Fig.5.14 and Fig.5.17, the radial force fluctuates with the rotor angular positions. Taken into account that the feedback control is easy to be realized in a linear system, this problem may be solved by feedback control. Therefore, we need to investigate what the relationship is between the radial force and control current with a coefficient k.

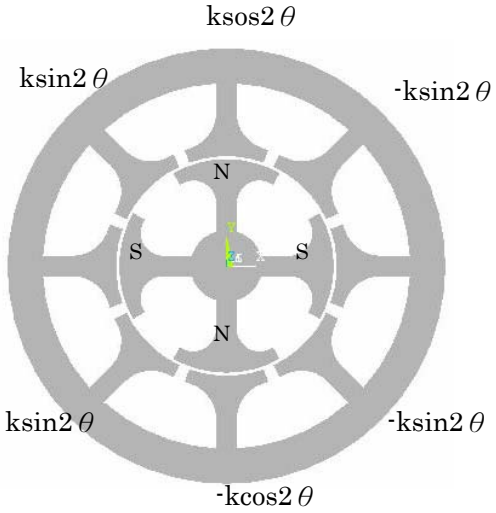

Fig.5. 19 Radial force control current arrangement with constant k

The investigation is conducted by the control current arrangement given in Fig.5.19. k

is a multiplying constant to the control currents. Changing the constant k from 0 to 1, with the incremental value being 0.2, the radial forces in x and y directions Fx and Fy as well as the torques with the changing of rotor angular positions have been computed using FEM. The results of radial forces are presented in Fig.5.20-Fig.5.22. The radial forces in y direction versus the constant k are shown in Fig.5.23.

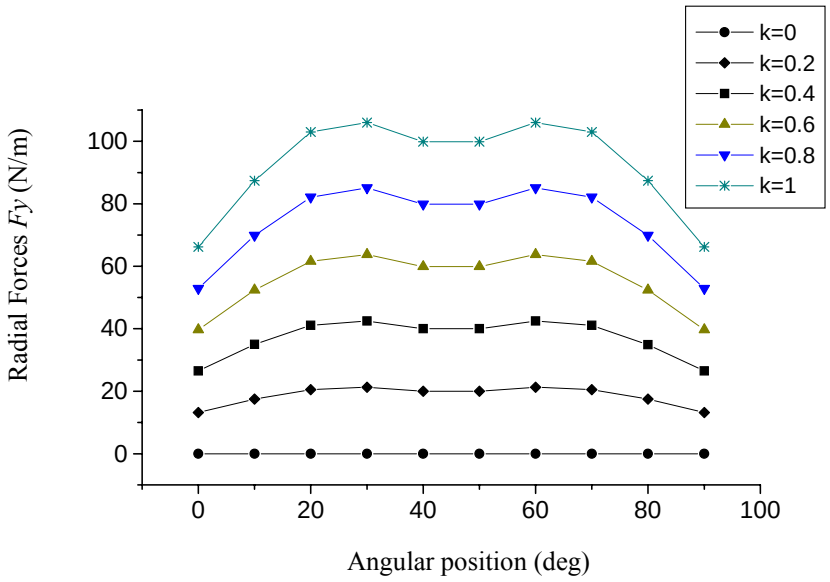

Fig.5. 20 Radial forces in Y direction versus angular position with constant k

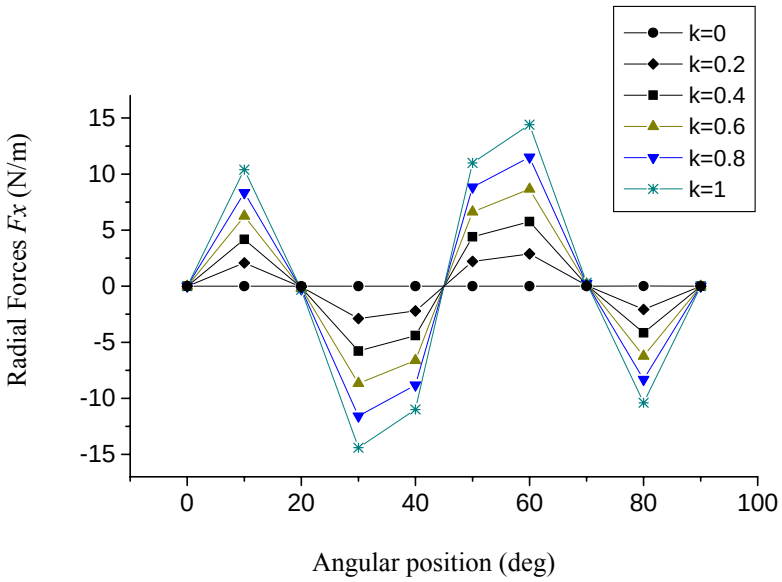

Fig.5. 21 Radial forces in X direction versus constant k

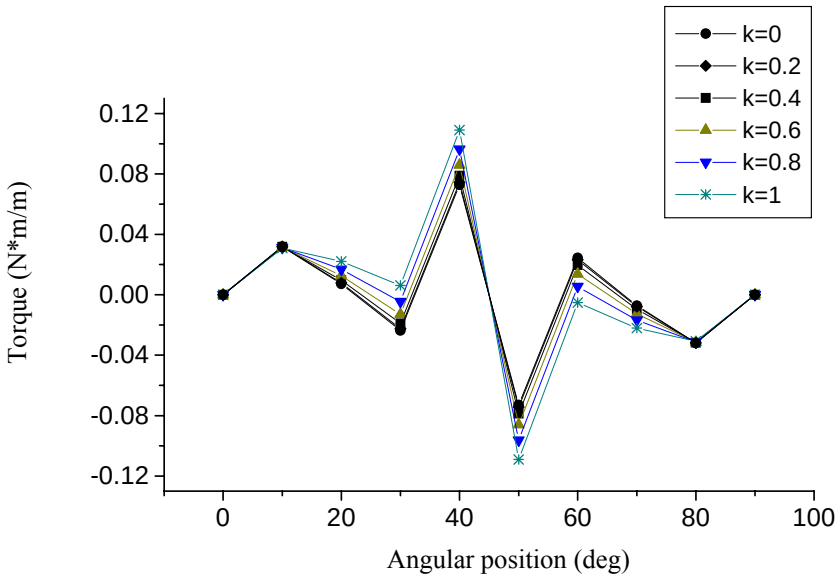

Fig.5. 22 Torque with different constant k

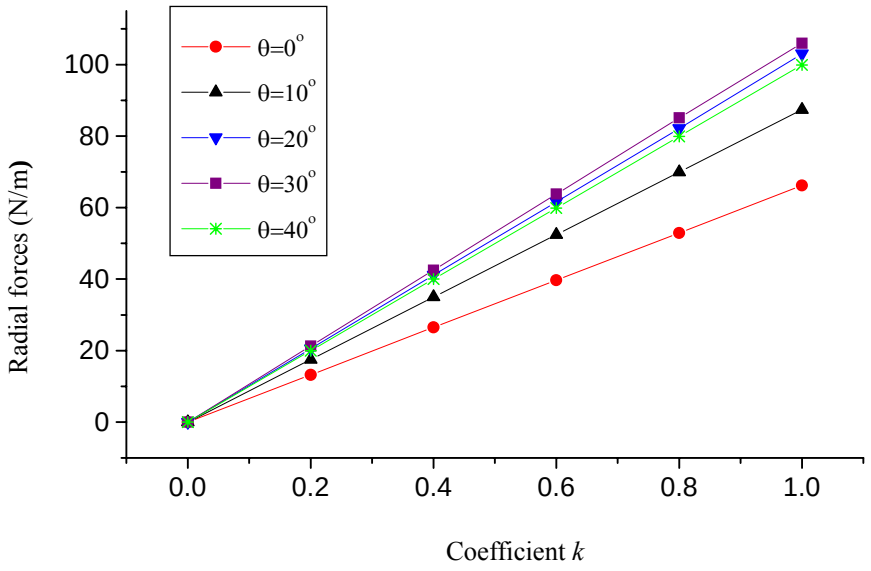

Fig.5. 23 Radial forces with constant k

From these figures, it can be seen that the radial force and the coefficient k have a linear relationship. Therefore, the feedback control method can be adopted to regulate the radial force.

5.3 Summary and Remarks

A new shape of test bearingless motor with rectifier rotor coil has been designed. In order to increase the radial force and rotation torque, the shapes of rotor and stator poles have been designed to be like unfolded fans to increase the facing area between the rotor and stator poles. FEM analysis method has been used to compare the differences between the old test machine and the new one. The results verify that the new test machine can generate a larger radial force and rotation torque, and no zero torque position exists.

For the new shape of bearingless motor with rectifier rotor coil, the radius of the rotor is determined to be 60 mm for the easiness of treatment. Then the optimum rotor tooth size is decided by comparing the torques when the rotor tooth is shorter, equal and

longer than the stator tooth, and a tradeoff consideration for the tooth size that can generate relatively larger torque and radial force has been chosen.

Based on the new configuration of bearingless motor with rectifier rotor coil, the realization of rotation and radial force strategy has been investigated by finite element method, and the feasibility has been verified preliminary. Furthermore, the analysis results indicate that there is no coupling between the motor and radial force function when this control strategy is used. And it will contribute to simplify the control system.

In addition, it has been validated that the output radial force has a linear relationship with the input control current, which means that the radial force can be easily regulated by feed back control method.

All the results indicate that the proposed bearingless motor with rectifier circuits can be realized. However, all of the results are obtained under ideal situation, so the experiments should be carried out to validate the feasibility, and the analysis results can give a direction for the experiments.

Chapter 6 Experimental Study for Prototype II

6.1 Mechanical Configuration

Based on the feasibility and preliminary control strategy investigated by FEM in Chapter 4, a prototype bearingless motor with rectifier rotor coil is designed, the test machine is shown in Fig.6.1. The configuration parameters are given in Table 3.

The radius of the rotor is determined as 60 mm., which is decided by easiness of treatment. The shape of the stator and the rotor is like an unfolded fan because of necessity of large area facing to each other, since the induced current must be generated by mutual inductance, which depends on the faced area.

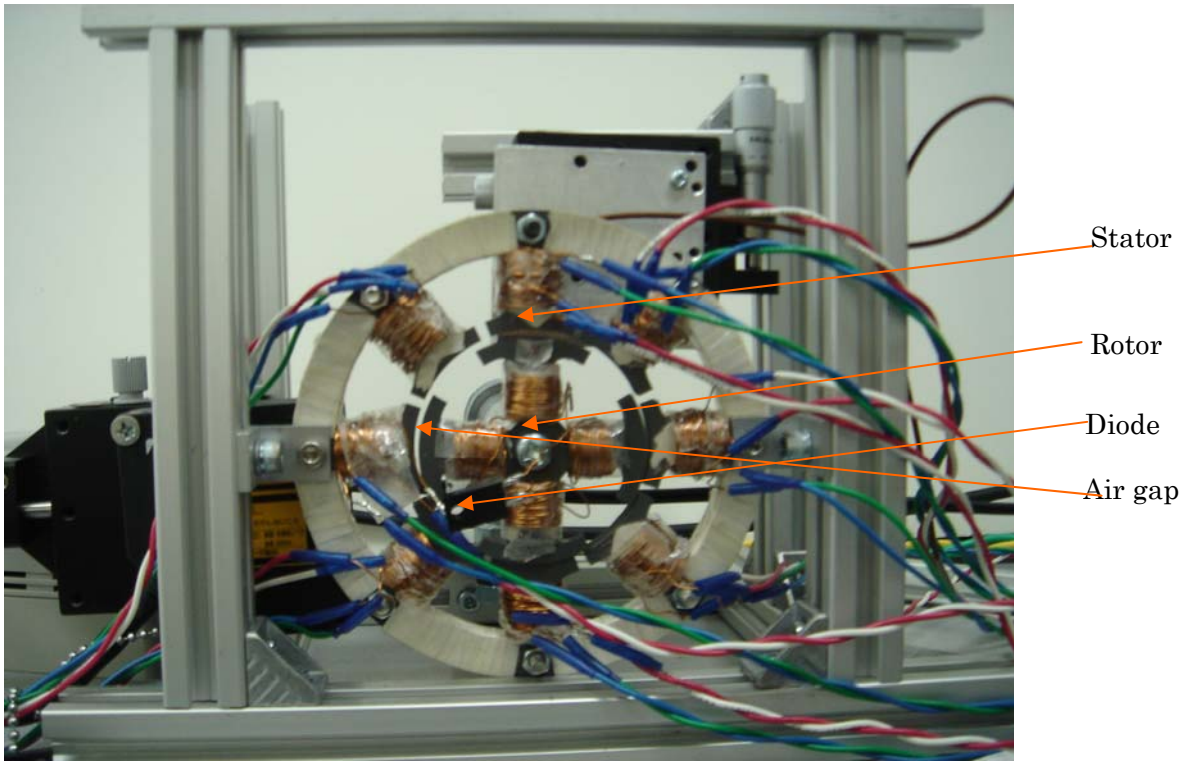

Fig.6. 1 Picture of prototype II

Table 3 Design parameters of prototype II

Average air gap	1mm
Turns of exciting coil	72
Turns of control coil	72
Turns of rotor coil	70
Outer diameter of stator	120mm
Outer diameter of rotor	59mm

6.2 Characteristics of Rectified Bearingless Motor

Based on the analyses in Chapter 4, the prototype II of the bearingless motor with rectifier circuit coil has been fabricated. The A-phase stator exciting winding configuration is shown in Fig.6.2. The exciting winding *N*e consists of four coils connected in series. The control coil connects with the opposing one in series too. As illustrated in Fig.6.2, cos2θ and sin2θ are the control current arrangements for radial force control. The horizontal radial forces with respect to control currents have been measured when the exciting voltage is 26V, 8V and 0 V respectively, and the AC

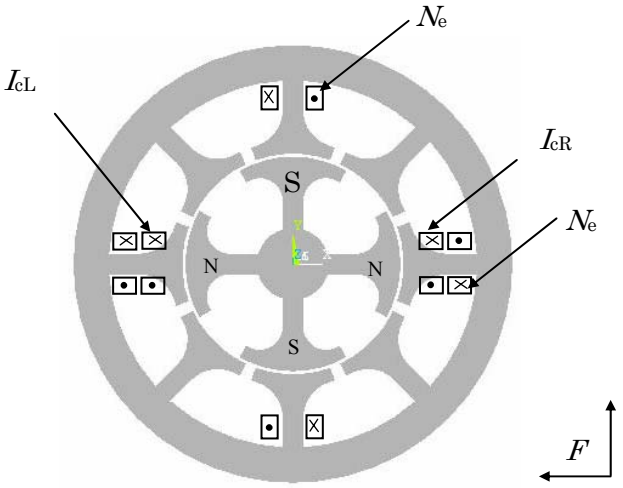

Fig.6. 2 Configuration of exciting and controlling winding

voltage frequency is 800Hz. Fig.6.3 presents the generated radial forces when only the control current *I*cL is applied. It can be seen that when the exciting voltage is zero, the direction of the radial force does not change with the control current. However, when the exciting voltage shown in Fig.6.2 is applied to the exciting winding, the negative force is produced as the control current *I*cL changes its direction, which verifies that the existence of rectified coil makes the rotor possess a fixed polarity and have the characteristic of a permanent magnet.

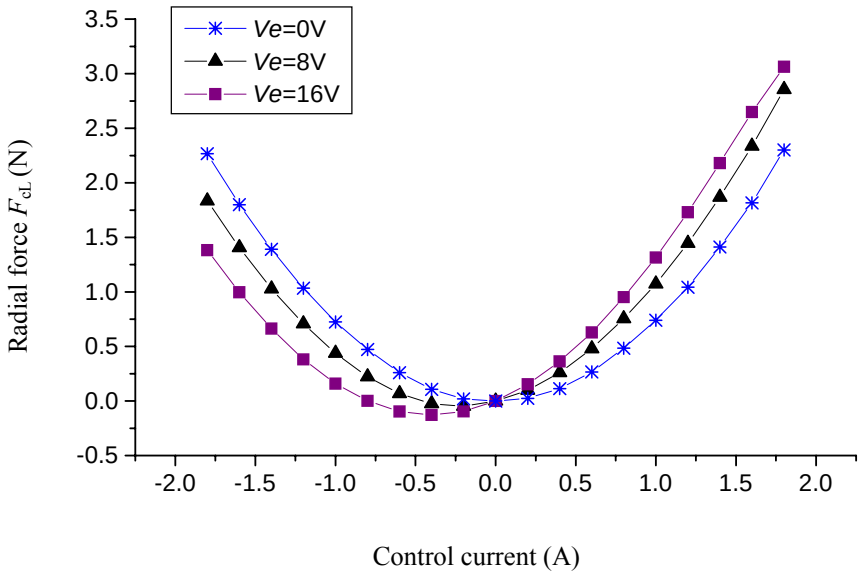

Fig.6. 3 Radial force when just control current I_{cL} is applied

The radial forces have also been measured when only the control current I_{cR} is applied, and the results are shown in Fig.6.4. When both the control currents I_{cL} and I_{cR} are applied to the control current coils at the same time, the measured radial forces are shown in Fig.6.5. It can be seen that these values are rightly equal to the summation of F_{cL} and F_{cR}.

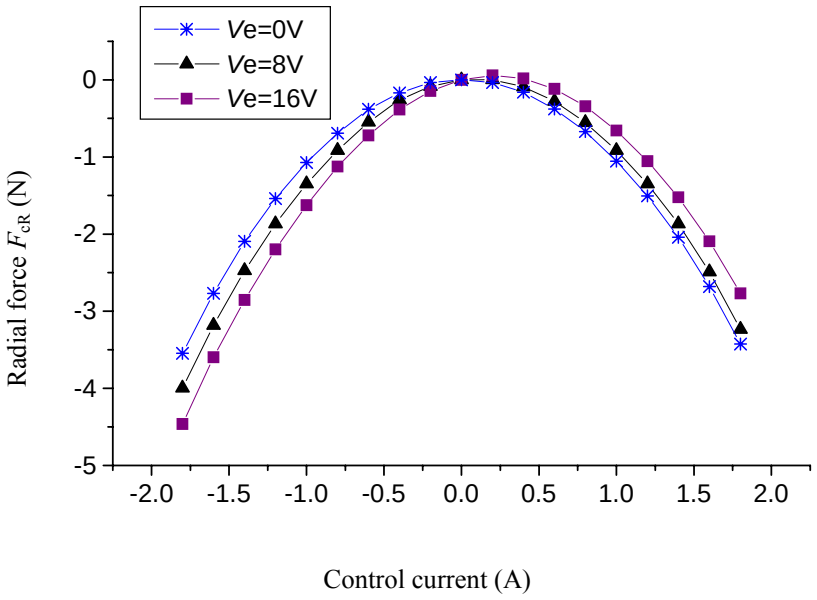

Fig.6. 4 Radial force when just control current I_{cR} is applied

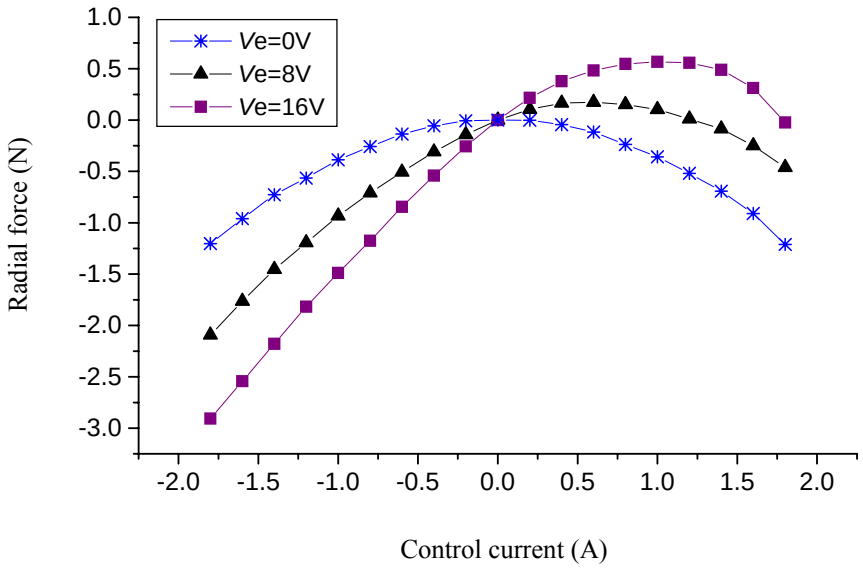

Fig.6. 5 Radial forces when both I_{cL} and I_{cR} are applied

However, from the experiment, it is also found that the induced magnetic flux is not strong enough when the exciting voltage is 16 volts. Therefore, the exciting voltage is changed to AC 26 volts, and frequency 900Hz. While the control current arrangement for the vertical radial force is shown in Fig.6.6 in black letters, the control current arrangement for the horizontal radial force is shown in Fig.6.6 in blue ones. When the rotor is located in the position shown in Fig.6.6, the angle θ is equal to zero.

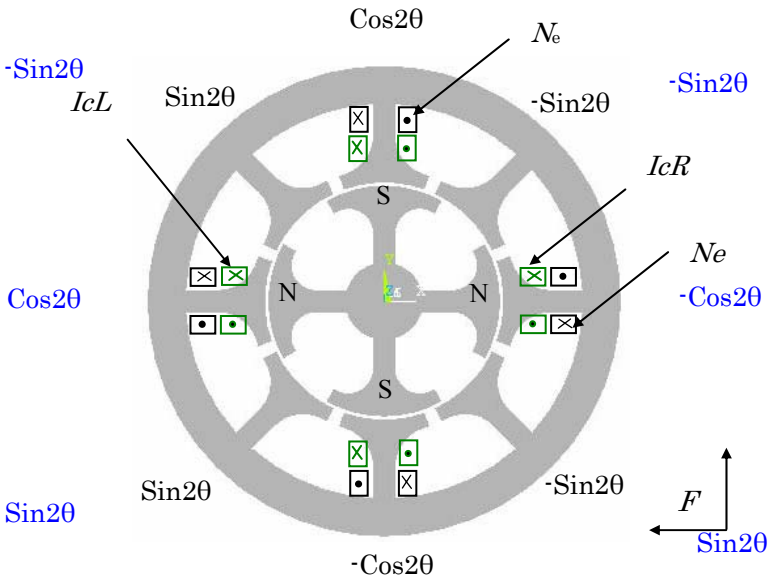

Fig.6. 6 Configuration of exciting and control coils

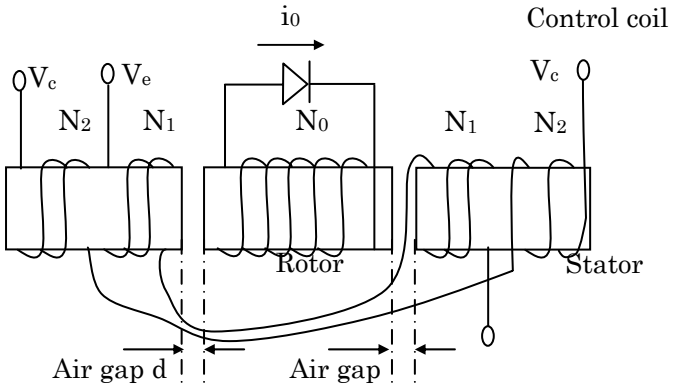

Fig.6. 7 Configuration of exciting and control coils in detail

First, only the exciting voltage and horizontal control current are applied, the detailed schematic of winding connection is shown in Fig.6.7. The radial forces have been measured when the rotor is located at different positions. The results are shown in Fig.6.8 and Fig.6.9.

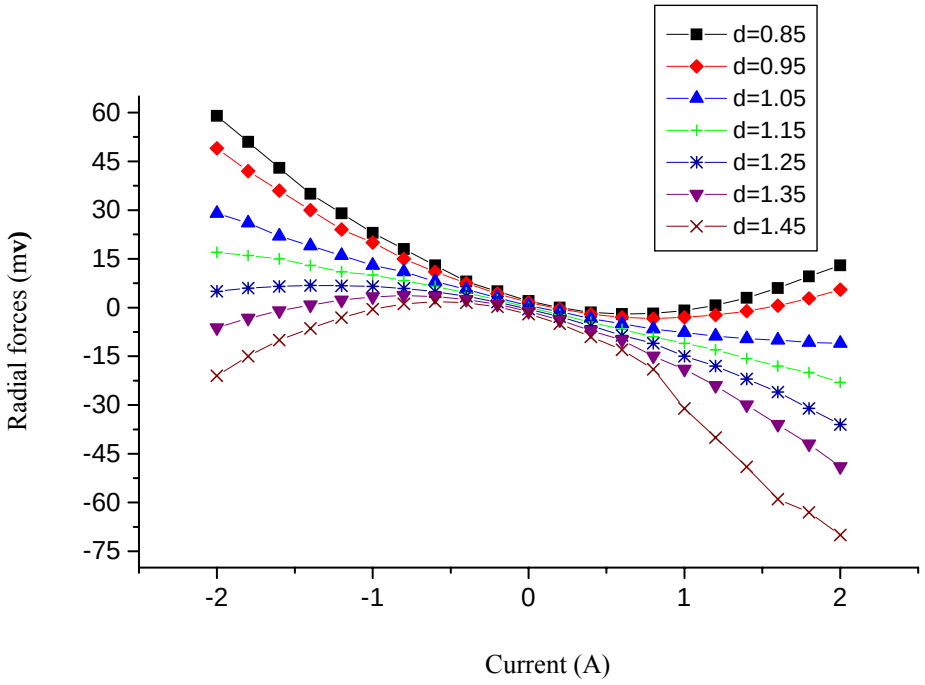

Fig.6. 8 Radial forces with respect to control current

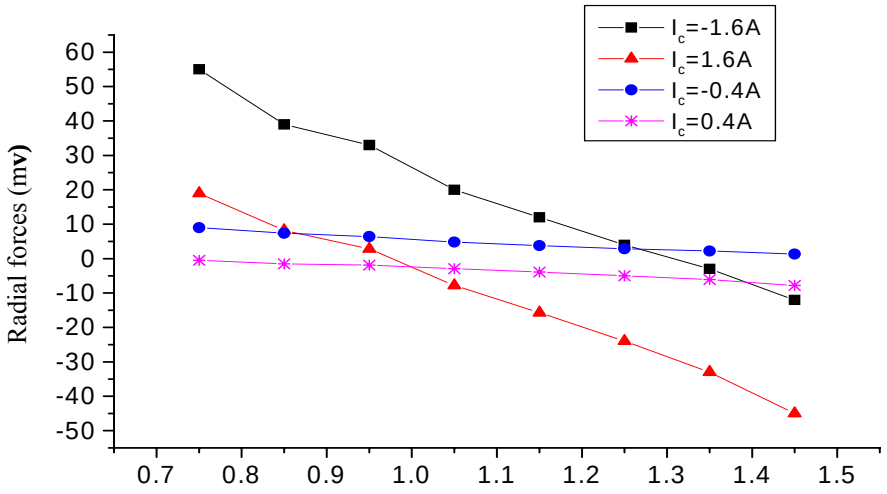

Fig.6. 9 Radial forces with respect to air gap

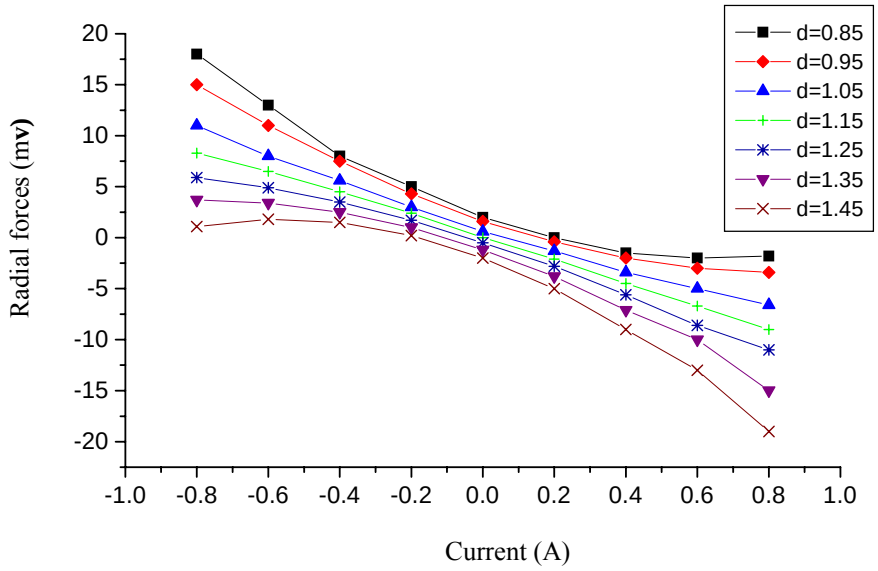

Fig.6. 10 Radial forces with respect to control current

From Fig.6.8, it can be seen when the air gap *d* is equal to 1.05mm and 1.15mm, the generated radial force almost has a linear relationship with the control current, that is to say, when keeping the rotor air gap range between 1.05mm and 1.15mm, a linear feed back control method can be used to maintain the rotor at its balanced position.

Fig.610 gives the amplification of Fig.6.8. How the radial forces change with the control current can be seen much more clearly in this figure.

6.3 Implementation of Rotor Position Control

Based on the above analyses, the exciting AC voltage of 26 volts and 900Hz is applied, just as shown in Fig.6.6. Linear PD controller is used to regulate the control current both in horizontal and vertical directions. Fig.6.10 is the schematic of control strategy for the vertical direction force, and the control strategy for the horizontal direction force is the same.

Because the electromagnetic force of the rotor is a function of the current going through the control coil, the modulation of the control current can realize the movement

and position of the rotor. The control system is implemented digitally using a high-speed digital signal processor board. The control block diagram is shown in Fig. 6.10.

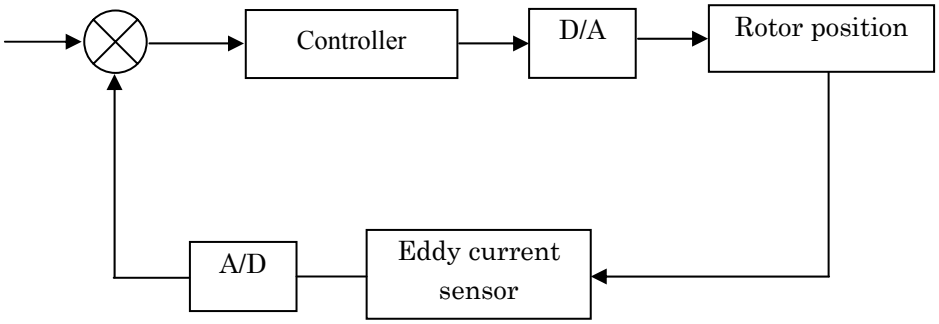

Fig.6. 11 Rotor position control for vertical direction

Firstly, the rotor position is measured with the eddy current sensor, then the measured value is feedback to DSP controller, the feedback signal is compared with the given value (here is the rotor position), then a control coil current is output to keep the rotor locating at the balance position.

The experiment results are given in Fig.6.11 and Fig.6.12. After the rotor got its balance, we input a disturbance signal, and it can be seen that the rotor will change its position correspondingly.

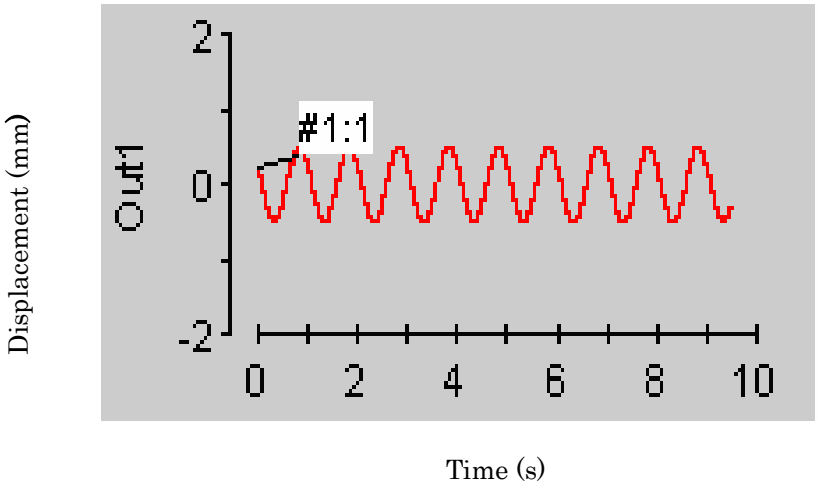

Fig.6. 12 Reference input signal

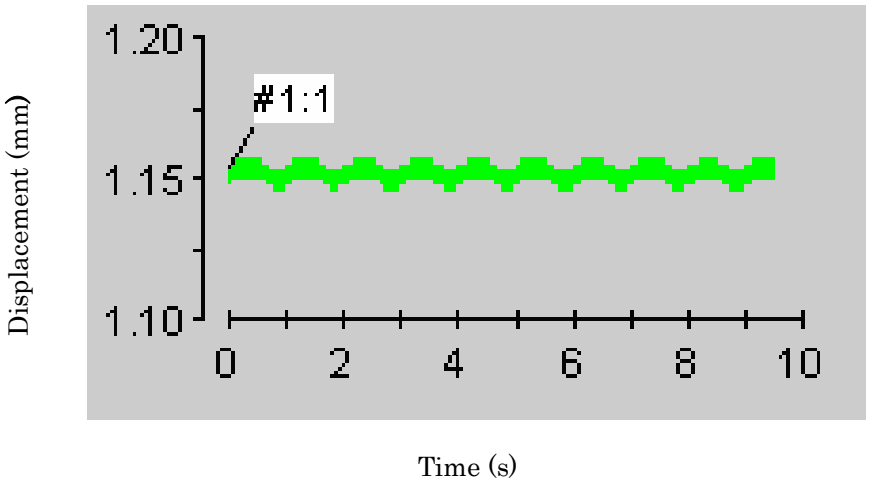

Fig.6. 13 Rotor response trajectory

6.4 Implementation of Motor Rotation

For the development of bearingless motor with rectifier circuit, firstly, the rotor rotation is tested when the rotor center is fixed to a mechanical bearing, and the results show that the rotor can work just as we supposed like a permanent magnet stepping motor.

6.4.1 FEM analysis

Firstly, the performances of the rotor rotation are analyzed using FEM, that is keeping the rotor poles magnetized by DC current, and keeping the rotor angular position of the control coil current θ equal to 22.5^{o}, e.g. keeping the control current constant, the control current arrangement is shown in Fig.6.13, then rotating the rotor, how the torque changing with the rotating angle is computed, the results are shown in Fig.6.14.

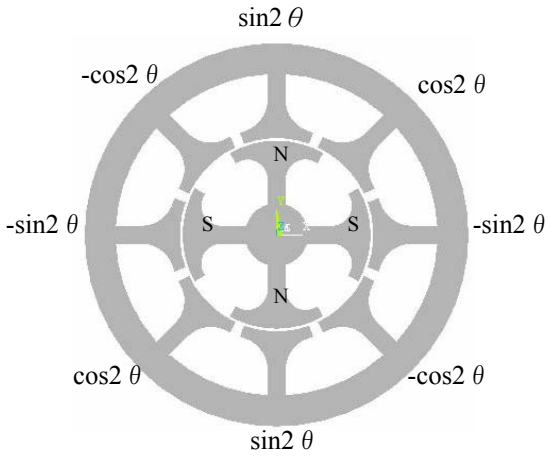

Fig.6. 14 Control current arrangement for the torque production

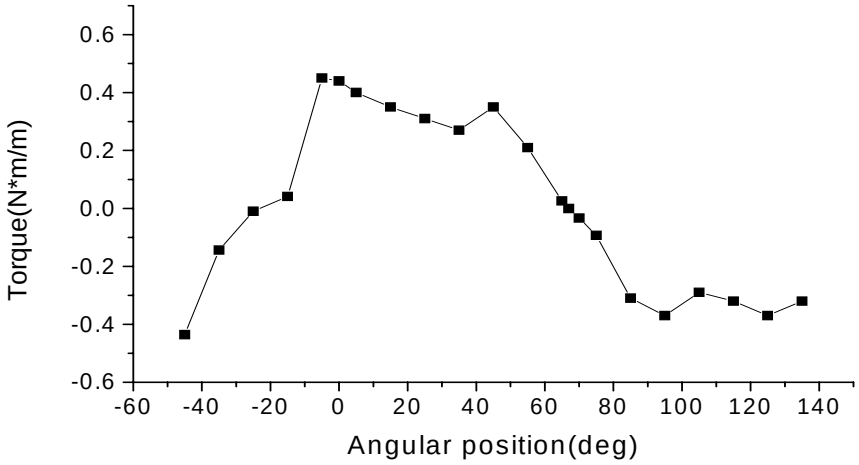

Fig.6. 15 Torque versus the rotor angular position

From Fig.6.14, it can be seen that when the rotor rotating angle θ changing from -45° to 145°, that exactly is the half rotation of the rotor, it is found that the rotor got its balanced position when the rotation angle equal to 67.5°. At this point, with the increasing of the rotor rotation angle, the rotor torque changed its direction. The angle θ equal to 65 and 70 are also computed, which are the points nearing the balanced position, the results present that the slope is sharp, that means the opposing torque is large.

Taken into account that θ equal to 45° is another typical position, the rotation torque is computed when the control current is fixed. The control current arrangement is shown

in Fig.6.15, and θ is fixed to equal 45°, the results are shown in Fig.6.16.

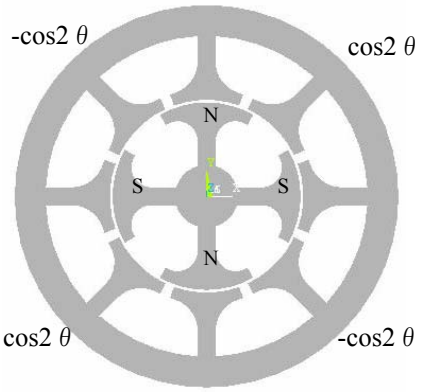

Fig.6. 16 Control current arrangement for the torque production

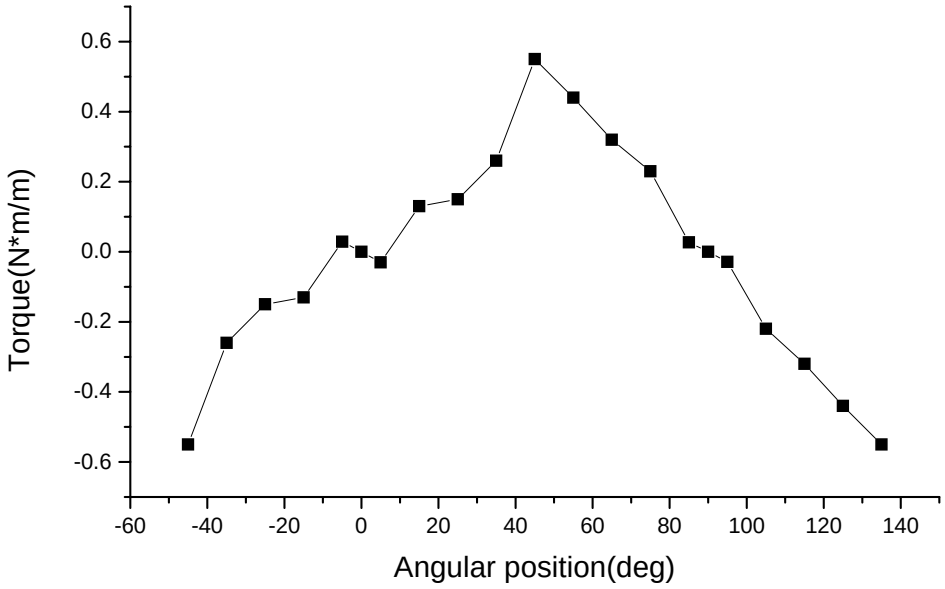

Fig.6. 17 Torque versus the rotor angular position

From Fig.1.16, it can be seen that when the rotor angular position is equal to 90°, the

rotor got its balanced position. The points θ equal to 85 and 95 are calculated also, results show that, the slope is not large comparing with the former situation, with means that the opposite torque is not very strong, but it still can returned to the balanced position.

For these two situations, the balanced angles are equal to $45^{o}+\theta$.

6.4.2 Experimental verification

The rotor rotation has been verified by experiment, the rotor can be rotated just like a permanent magnet stepping motor.

6.5 Summary and Remarks

According to the FEM analyses, the prototype of bearingless motor with rectifier rotor coil is fabricated, and some variable relationships have been investigated. Based on these results, a control system based on DSP controller is used to modulate the control current of control coil to realize the rotor position control both in horizontal and vertical directions. It has been verified that the rotor levitation can be realized.

From the experiment, it is still found that if the rotor deviates from the center position more than 0.1mm, the rotor will be out of balance. Some control methods should be considered to improve the system stability.

Chapter 7 Conclusions

For the proposed bearingless motor with rectifier circuit, the principle has been introduced firstly, then its feasibility is verified by numerical simulation. The fundamental characteristics of the proposed bearingless motor have been investigated by means of FEM and experiments. Based on the Prototype II, the strategies for radial force and rotation torque control have been studied by FEM, and the rotor position control has been implemented preliminary.

Chapter 1 gives an overview about bearingless motor. Bearingless motor is an electromagnetic machine that has the functions of electric motor and active magnetic bearing, and possesses the capabilities of both a magnetic bearing and a motor. Sometimes it is also called self-bearing motor or integrated motor bearing. There are some special applications for bearingless motors, such as high speed drives and generators, bioreactors and semiconductor-technology, biomedical products e.g. artificial hearts, respiratory support equipment, flywheel drives and generators. The rapid development of the related technologies such as power electronics, vector control theory and digital signal processing greatly contributes to the realization of bearingless machines. Then, the bearingless motor types, winding structures and configurations that have been developed are summarized. Finally, a new type of bearingless motor with rectifier rotor coil is proposed.

In the followed chapter, the principle of the proposed bearingless motor with a rectifier circuit is introduced in detail. In the proposed brearingless motor structure, a rotor with rectified circuit coil is used to replace the permanent magnet rotor of stepping PM motor. Therefore, this bearingless motor will inherit all the performances of permanent magnet motor. Furthermore, the rotor mechanical strength will be improved compared with permanent magnet, because the material of rotor is silicon steel sheet, and the reluctance can be decreased. Besides, it can overcome the deficiency of demagnetization. As compared with the reluctance motors, the problem such as rotor vibration can be restrained. In addition, the motor contains a decoupling structure of

torque and radial force, which will simplify the control system.

The feasibility for the proposed bearingless motor structure has been verified by means of numerical simulation. A simple test instrument has been built. Both simulation and experiment results prove that the rotor can be magnetized to possess the performance of permanent magnet. Furthermore, the relationships between all of the variables such as induced current versus air gap, flux density versus exciting voltage, etc. have been measured. These results will provide an instructive direction for the following design work.

In Chapter 3, based on the prototype I, the characteristics such as the induced current with winding turns, radial force versus control current, torque and radial force versus the rotor angular position, have been investigated. Following these preknowledge, we tried to realize the rotor rotation, but the rotor was failed to rotate like a stepping motor just as we supposed. From the FEM analyses, the flux distribution shows that when the rotor poles align with the stator poles, there are only few flux lines flowing between the neighbored stator and rotor poles, The FEM calculation results also indicate that the torque value is very small at that moment, which causes a zero torque position. Therefore, a new shape of bearingless motor is desired which can overcome the deficiency of this prototype.

For Chapter 4, the prototype II is designed. In order to increase the magnitude of radial force and rotation torque, the induced current must be generated by mutual inductance, which depends on the faced area to the shape of rotor, so the stator poles have been designed to be like an unfolded fan to increase the facing area between the rotor and stator tooth. FEM analysis method has been used to analyze the characteristic of this test machine. The results show that the new test machine can generate a larger radial force and rotation torque, and no zero torque position.

For the new shape of bearingless motor with rectifier rotor coil, the radius of the rotor is determined for the easiness of treatment. Then the optimum size of rotor tooth is determined by comparing the torques when the rotor tooth is shorter, equal and longer than the stator tooth, and a tradeoff consideration for the tooth size with which the motor can generate relatively larger torque and radial force has been chosen.

Based on the new configuration of bearingless motor with a rectified rotor coil, the

realization of rotation and radial force strategy has been investigated by finite element method, and the feasibility has been verified preliminary. The analysis results indicate that there is no coupling between the motor and radial force function. Therefore, when the proposed control strategy is used, it will contribute to simplify the control system.

In addition, it has also been validated that the output radial force has a linear relationship with the input control current, which means that the radial force can be easily regulated by feed back control method.

All the results indicate that the proposed bearingless motor with a rectified circuit can be realized. However, all of the results are obtained under ideal conditions, so experiments should be carried out to validate the feasibility. The analysis results will give a direction for the experiments.

In Chapter 5, using the prototype II, a control system based on DSP controller is constructed.

Firstly, the characteristics of radial force change with the air gap and control current were measured, and it is found that when the air gap is equal to 1.05mm or 1.15mm, the generated radial force almost has a linear relationship with the control current. This indicates that when the air gap between the rotor and stator changes from 1.05mm to 1.15mm, a linear control method can be used to keep the rotor balance.

The electromagnetic force of the rotor is a function of the current which goes through the control coil. The modulation of the control current can realize the movement of the rotor position. The control system is implemented digitally using a high-speed digital signal processor board. An eddy current sensor is used to measure the rotor displacement, then this signal is fed back to the controller, and the DSP controller compares the feedback signal with the given value of the rotor position, then the control coil current is output to keep the rotor being at the balance position. The rotor levitation has been successfully realized.

From the experiments, it is found that if the rotor deviated from the center position more than 0.1mm, the rotor will be out of balance. Some control methods, e.g. adaptive control method, may be considered to improve the system stability.

From the numerical and FEM analyses, the results show that the proposed bearingless

motor with rectifier rotor coil can be realized. Moreover, the feasibility has been verified by the experiment results of rotor levitation. Certainly, there are many jobs still to be done for the complete implementation of the proposed bearingless motor with rectifier circuit coil.

So far, for the proposed bearingless motor, only the rotor levitation has been realized, and the stability of the system still needs to be improved, and the robustness should be strengthened. Therefore, some issues in the thesis should be further investigated. The analysis on the achievable performance PD controller is used. Maybe some other control schemes such as H_∞ or adaptive control method can also be tried to investigate how the hardware components constrain the system performance.

The followed job is to realize the rotor rotation by experiment.

Acknowledgement

First, I would like to express my sincere appreciation to my supervisor, Oka Koichi Sensei, for his guidance throughout my thesis work. He has been leading me in the direction of the research, both practical and theoretical relevance. His ideas, suggestions and constructive comments have helped me a great deal.

Special thanks give to Oka family, who always treat me with warmhearted kindness.

I want to thank Hironobu Aratani, a graduate student in Oka lab. He always speaks little but do much. Without his support, the experiment would not have been completed.

I also thank all of the students in Oka lab. They always give me warm help whenever I need.

Last, but not least, I want to give my appreciation to my husband, Xiang Qingchun. His love and encouragement have been of special importance to me.

References

[1] Magnetism and Earnshaw's Theorem. http://www.mathpages.com/home/kmath240/kmath240.htm

[2] S. Akishita, T. Morimura, and S. Hamaguchi, "Vibration control of magnetically suspended flexible rotor by the use of optimal regulator," 2nd international symposium on magnetic bearing, July 147-154, 1990, Tokyo, Japan

[3] Beams JW, Young JL, Moore JW. (1946) The production of high centrifugal fields. J. Appl. Phys., 886-890.

[4] Larsonneur R. (1990) Design and control of active magnetic bearing system for high speed rotation. Diss. ETH Zurich Nr. 9140.

[5] Loesch F. (2001) Identification and automated controller design for active magnetic bearing systems. Diss. ETH Zurich Nr. 14474.

[6] Noh, M.D.; Seong-Rak Cho; Jin-Ho Kyung; Seung-Kook Ro; Jong-Kweon Park Mechatronics, "Design and implementation of a fault-tolerant magnetic bearing system for turbo-molecular vacuum pump" IEEE/ASME Transactions on Volume 10, Issue 6, Dec. 2005 Page(s): 626 – 631.

[7] G.F. Weston "Developments in high-vacuum pumps." 1984 Physics in Technology 15 37-44

[8] U.J. Bichiler, " A low noise magnetic bearing wheel for space application," 2nd international symposium on magnetic bearing, July 12-14, 1990, Tokyo, Japan.

[9] G. Genta, L. Mazzocchetti, and E. Rava, " Magnetic suspension for a turbomolecular pump, " 2nd international symposium on magnetic bearing, July 65-72, 1990, Tokyo, Japan.

[10] M. Ota, S. Andoh, and H. Inoue, "Mag-lev semiconductor wafer transporter for ultra-high-vacuum environment" 2nd international symposium on magnetic bearing, July 109-114, 1990, Tokyo, Japan.

[11] K. Nonami and H. Yamaguchi, "Active vibration control of flexible rotor for high order critical speeds using magnetic bearings," 2nd international

symposium on magnetic bearing, July 155-160, 1990, Tokyo, Japan.

[12] Swann, Michael K. “Magnetic bearings: Fifty years of progress.” In NASA. Langley Research Center, Magnetic Suspension Technology Workshop p 19-38 (SEE N93-27554 10-18), 1993.

[13] P.K. Hermann, “A radial active magnetic bearing,” Londen Patent No.1 478 868, 20 Nov. 1973.

[14] P.K. Hermann, “ A radial active magnetic bearing having a rotating drive,” Londaon Patent No.1 500 809, 9 Feb. 1974.

[15] P. Meike, G. Flachenecker, “Electromagnetic drive assembly for rotary bodies using a magnetically mounted rotor,” United States Patent NO.3 988 658, July 29, 1974.

[16] T. Higuchi, “Magnetically floating actuator having angular positioning function,” United States Patent No.4 683 391, 12 March 1985.

[17] R. Bosch, “Development of a bearingless electric motor,” ICEM, PP 373-375, 1988

[18] A. Chiba, T. Deido, T. Fukao and M.A. Rahman, “An analysis of bearingless AC motor,” IEEE Trans. On Energy conver, vol.9, No.1, PP. 61-68, Mar. 1994.

[19] R. Schob, J. Bichsel, “Vector control of the bearingless motor,” Ismb, PP. 327-332, Zurich 1994.

[20] M. Ooshima, A. Chiba, T. Fukao, M.A. Rahman, “ Design and analysis of permanent magnet-type bearingless motors,” IEEE trans., Ind, Elec., Vol-43, No.2, pp.292-299, Apr. 1996.

[21] A. Chiba, S, Onoya, T. Kikuchi, M. Ooshima, S. Yiyazawa, F. Nakamura, T, Fukao, “ An analysis of a prototype permanent-magnet bearingless motor using finite element method,” ISMB Kanazawa, pp. 351-356, Aug. 1996.

[22] K. Inagaki, A. Chiba, M.A. Rahman, T. Fukao, “ Performance characteristics of inset-type permanent magnet bearingless motor drives,” IEEE PES. WMC, CDROM Singapore, Jan. 2000.

[23] A. Chiba, D.T. Power, M.A. Rahman, “Analysis of no-load characteristics of a bearingless induction motor”, IEEE Trans. On IAS, Vol.31, No.1, pp.77-83, Jan./Feb. 1995.

[24] Akira Chiba, Tadashi Fukao, “The state of the art in developments of bearingless drives,” 産業応用部門誌　２００１年 Vol. 121-DJULY 2001 Volume 121-DNumber 7

[25] A. Chiba, D.T. Power,M.A. Rahman, “Characteristics of a bearingless induction motor”, IEEE Trans. On Mag., pp.5199-5201, Sep., 1991.

[26] S. Nomura, A. Chiba, F. Nakamura, K. Ikeda, T. Fukao, M.A. Rahman, “A radial position control of induction type bearingless motor considering phase delay by the rotor squirrel cage”, IEEE PCC, pp.438-443, Japan, Apr. 1993.

[27] A. Chiba, T. Fukao, “The maximum radial force of induction machine type bearingless motor using finite element analysis”, ISMB, pp.333-338, Aug. 1994.

[28] Y. Takamoto, A. Chiba and T. Fukao, “Test results on a prototype bearingless induction motor with five-axis magnetic suspension”, IPEC, Vol.1, pp.334-339, Yokohama, Apr.1995.

[29] A. Chiba, R. Miyatake, S. Hara and T. Fukao, “Transfer characteristics of radial force of induction-type bearingless motors with four-pole rotor circuits”, ISMB, pp.319-325, Japan, Aug. 1996.

[30] A. Chiba, R. Furuichi, Y. Aikawa, K. Shimada, Y. Takamoto, T. Fukao. “Stable operation of induction-type bearingless motors under loaded conditions”, IEEE Trans on IAS Vol.33, No.4, pp.919-924, July 1997.

[31] A. Chiba, T. Fukao, “Optimal design of rotor circuits in induction type bearingless motors”, IEEE Trans. on Mag, Vol.34, No.4, pp.2108-2110, Jul.1998.

[32] A.O. Salazar, W. Dunford, R. Stephan, E. Watanabe, “A magnetic bearing system using capacitive sensors for position measurement”, IEEE Trans. on Magnetics, Vol.26 No.5, pp.2541-2543, Sept. 1990.

[33] A.O. Salazar, R. M. Stephan, “A bearingless method for induction machine”, IEEE Trans. on Magn., Vol.29, No.6, pp.2965-2967, Nov. 1993.

[34] J. Santisteban, A.O. Salazar, R.M. Stephan, W.G. Dunford, “A bearingless machine-an alternative approach”, ISMB, pp.345-349, Japan, 1996.

[35] J.A Santisteban, R.M. Stephan, “Analysis and control of a loaded bearingless machine”, IEEE Trans. Mag., Vol.35, No.5, pp.3997-4000, Sep. 1999.

[36] K.B. Yahia, G. Henneberger, “Development of bearingless induction motor”, MOVIC, Zurich, Switzerland, Vol.3, pp.1083-1087, Aug. 1998.

[37] T. Gempp, R. Schob, “Design of a bearingless canned motor pump”, ISMB, pp.333-338, Kanazawa, Japan, 1996.

[38] T. Satoh, S. Mori, M. Ohsawa, “Study of induction type bearingless canned motor pump”, IEEJ IPEC, pp.389-394, Tokyo, Japan, 3-7, Apr.2000.

[39] M. Takemoto, K. Shimada, A. Chiba and T. Fukao, “A design and characteristics of switched reluctance type bearingless motors”, Inter. Sym. On Mag. Suspension Tech., pp.49-63, Japan, May. 1998.

[40] M. Takemoto, H. Suzuki, A. Chiba, “Improved analysis of a bearingless switched reluctance motor”, IEEE transactions on industry applications, Vol.37, No.1, Jan/Feb 2001.

[41] M. Ooshima, S. Miyazawa, T. Deido, A. Chiba, F. Nakamura, T. Fukao, “Characteristics of a permanent magnet type bearingless motor,” IEEE Trans. On IA, vol.32, No.2, pp. 363-370, Mar. 1996.

[42] Y. Okada, T. Ohishi, K. Dejima, “ Levitation control of permanent magnet type rotting motor”, Proc. of Magnetic Bearing, Magnetic Drives and Dry Gas, pp. 157-166, Alexandria, VA. USA July 1992.

[43] T. Ohishi, Y. Okada, S. Miyamoto, “ Levitation control of IPM type rotation motor ”, ISMB, pp. 327-332, Kanazawa, Japan, 1996.

[44] Y. Okada, K. Shinohara, S. Ueno and T. Ohishi, “ Hybrid AMB type self bearingless motor,” Int. Symp. Magnetic Bearing, pp. 497-506, 1998.

[45] W. Amrhein, S. Silber, “ Single phase PM motor with integrated magnetic bearing unit”, ICEM’98, Vol.3, pp. 1277-1282, 1998.

[46] W. Amrhein, S. Silber, “ Bearingless single-phase motor with concentrated full pitch windings in interior rotor design”, ISMB, pp. 486-496, 1998.

[47] U. Bikle and K. Reichert, “ Lateral force in a bearingless interior-type permanent-magnet synchronous machine”, ICEM, Vol.3, pp. 1156-1160, 1998.

[48] R. Schob, N. Barletta, M. Weber, R. von Rohr, “ Design of a bearingless bubble

bed reactor," ISMB, pp.507-516, 1998.

[49] J.F. Charpentier and G. Lemarquand, "A comparative analysis of permanent magnet-type bearingless synchronous motor for fully magnetically levitated rotor," Jour. Of Applied Phys., Vol.83, No.11, pp.7121-7123, Jun. 1998.

[50] C. Barthod and G. Lemarquand, "Design of an actuator being both a permanent magnet synchronous motor and a magnet suspension," IEEE Trans. On Mag., Vol.34, No.4, pp.2105-2110, Jul. 1998.

[51] F. X. Wang, L. Y. Xu, "Design and analysis of a permanent magnet motor integrated with journal bearing", IEEE Proc. of IAS 1997.

[52] W. Amrhein, S. Silber, K. Nenninger, G. Trauner, M. Reisinger, "Developments on bearingless drive technology", 8th international symposium on magnetic bearing Aug. 26-28, Mito, Japan, 2002.

[53] A. Chiba, M.A. Rahman and T. Fukao, "Radial force in a bearingless reluctance motor", IEEE Trans. on Mag., Vol.27, No.2, pp.786-790, Mar. 1991.

[54] A. Chiba, M. Hanazawa, T. Fukao and M.A. Rahman, "Effects of magnetic saturatio on radial force of bearingless synchronous reluctance motors ", IEEE Trans. on IA, Vol.32, No.2, pp.354-362, March/April, 1996.

[55] S. Mori, S. Tadashi, M. Ohsawa, "Experiments on a bearingless synchronous reluctance motor with load", ISMB, Japan, pp.339-343, Sep. 1996.

[56] M. Haris, C. Michioka, Y. Toyoshima, O. Ichikawa, A. Chiba and T. Fukao, "Measurement of radial force constant of homopolar type bearingless motor", IEEJ IAS, Nat. Conv., 1997.

[57] O. Ichikawa, A. Chiba and T. Fukao, "Development of Homo-polar type bearingless motors", IEEE, IAS Annual Meeting Conference Record, pp. 1223-1228, Oct. 1999.

[58] M. A. Rahman, T. Fukao and A. Chiba, "Principles and developments of bearingless AC motors", IEEE Trans. on Energy Conver, Vol.9, No.1, pp.61-68, Mar. 1994.

[59] Y. Okada, S. Shimura, T. Ohishi, "Horizontal experiments on a PM synchronous type and induction type levitated rotating motor", IEEJ IPEC, pp.340-354, Yokohama-Japan, 1995.

[60] Y. Okada, K. Dejima, T. Ohishi, “Analysis and comparison of PM synchronous motor induction motor type magnetic bearings”, IEEE Trans. on IA, Vol.31, No.5, pp.1047-1053, Sep./Oct. 1995.

[61] K. Neninger, W. Amrhein, S. Silber, “bearingless single-phase motor with fractional pitch windings”, Seventh international symp. on magnetic bearings, aug. 23-25, 2000.

[62] K. Nenninger, W. Amrhein, S. Silber, G. Trauner, M. Reisinger, “Magnetic circuit design of a bearingless single-phase slice motor”, 8th internation symposium on magnetic bearing, Aug. 26-28, Mito, Japan, 2002.

[63] R. Schob, N. Barletta, “Principle and application of a bearingless slice motor”, V ISMB, pp.333-338, Kanazawa, Japan 1996.

[64] S. Ueno, H. Kanebako, T. Ohishi, K. Matsuda, Y. Okada, Y. Tanaka, T. Masuzawa, “Design of a self-bearing slice motor for a centrifugal blood pump”, VI ISMB, Boston, US, pp.143-151, 1998.

[65] H. Nakano, T. Tomita, M. Watada, S. Torii, D. Ebihara, “The experimental result of a bearingless permanent magnet disk-type motor”, 8th international symposium on magnetic bearing, Aug. 26-28, Mito, Japan, 2002.

[66] H. Suzuki, A. Suzuki, S. Sasaki and A. Ito, “Proto-model of novel contact-free disk suspension system utilizing diamagnetic material ”, 10th international symposium on magnetic bearings, aug. 2006.

[67] A. Chiba, K. Asami and T. Yamada, “Basic characteristics of an outer rotor consequent-pole bearingless drive”, 10th international symposium on magnetic bearings, Aug. 2006.

[68] T. Masuzawa, T. Kita, S. Ezoe, S. Ueno, Y. Okada, “Application of the combined motor-bearing to artificial hearts”, IPEC, pp.2120-2125, Japan, Apr. 2000.

[69] S. Silber, W. Amrhein, “Bearingless single-phase motor with concentrated full pitch wingdings in exterior rotor design”, ISMB, pp.476-485, 1998.

[70] Koichi Oka, “Bearingless motor with rectifier circuits,” 8th international symposium on magnetic bearing, Mito, Japan pp.271-275, August, 2002

[71] T. J. Bass, M. Ehsani, T. J. E. Miller and R. L. Steigerwald, “Development of a

unipolar converter for variable reluctance motor drives," IEEE Trans. Industry Appl. IA-23 (1987), pp. 545–553.

[72] D. E. Cameron, J. H. Lang and S. D. Umans, "The origin and reduction of acoustic noise in doubly salient variable-reluctance motors," IEEE Trans. Industry Appl. 28 6 (1992), p. 1250 November/December.

[73] P. J. Lawrenson, J. M. Stephenson, P. T. Blenkinsop, J. Corda, N N. Fulton, "Variable speed switched reluctance motors," IEE Proc., vol. 127, Pt. B, no. 4, July, 1980, pp. 253–265.

[74] G. S. Buja and M. I. Valla, "Control characteristics of the SRM drives-Part I: operation in the linear region," IEEE Trans. Industry Electron. 38 5 (1991), pp. 313–321 October.

[75] V. Ozbulur, M. O. Bilgiç, A. Sabanoviç, "Torque ripple reduction of a switched reluctance motor," in Proceedings of International Power Electronics Conference, IPEC'95, Yokohama, April 3–7, 1995, pp. 546–550.

[76] N. Matsui, N. Akao and T. Wakino, "High-precision torque control of reluctance motors," IEEE Trans. Industry Appl. 27 5 (1991), pp. 902–907 September–October.

Related Publications

Journals

[1] Li Chen, Koichi Oka, and Hironobu Aratani. “Analysis and Design of Bearingless Motor with Rectifier Circuit Coil Rotor,” Japanese Society of Applied Electromagnetics and Mechanics（JSAEM）(Accepted)

[2] Li Chen, Hironobu Aratani, and Koichi Oka. “FEM Analyses and Experimental Study of Bearingless Motor with Rectifier Circuits,” Transactions of the Institute of Electrical Engineers of Japan (IEEJ Trans.).（Submitted）

[3] 藤原 佑輔，崔 天時，陳 麗，岡 宏一, “永久磁石リニア駆動によるマニピュレーション -鉄球の回転制御 - Manipulation by Linear Driving Permanent Magnet -Rotation Control of Ironball”【日本 AEM 学会誌 Volume14 Number1 March 2006 (ISSN 0919-4452) p.126～p.131】

International Conferences

[1] Li Chen, Hironobu Aratani, and Koichi Oka. “FEM Analyses and Experimental Study of Bearingless Motor with Rectifier Circuits,” The 2006 International Conference on Electrical Machines and Systems, Nagasaki, Japan, November 20-23, 2006.

[2] Chen Li, Hironobu Aratani, and Koichi Oka. “Analysis of Bearingless Motor with Rectifier Circuits,” Tenth international symposium on magnetic bearings. Martigny, Switzerland, August 21-23, 2006. CD-ROM.

[3] Li Chen, Koichi Oka, and Hironobu Aratani. “Analysis and Design of Bearingless Motor with Rectifier Circuit Coil Rotor,”Asia-Pacific Symposium on Applied Electromagnetics and Mechanics (APSAEM2006). NSW, Australia, 20-21 July 2006.

[4] Koichi Oka, Noriaki Ninomiya, Li Chen, Yusuke Fujiwara. “Magnetic Suspension System with Variable Flux Path Mechanism Using Rotary Actuator.” Tenth International Symposium on Magnetic Bearings. Martigny, Switzerland, August 21-23, 2006. CD ROM.

[5] Koichi Oka, Yusuke Fujiwara, Chen Li. “Magnetic Suspension System with Variable Flux Path Mechanism,” 12th International Symposium on Interdisciplinary Electromagnetic, Mechanic & Biomedical Problems (ISEM2005), Bad Gastein, Austria, 2005.09.12～2005.09.14

[6] Koichi Oka, Yusuke Fujiwara, Tianshi Cui, Li Chen “Noncontact Spinning Mechanism Using Linearly Actuated Magnets” The Fifth International Symposium on Linear Drives for Industry Applications, September 25～28, Kobe-Awaji, Japan 2005 pp.552-555.

Domestic Conferences

[1] 陳　麗, 荒谷　広宣, 岡　宏一　“整流コイルをロータに持つベアリングレスモータの開発”- 平成 19 年電気学会全国大会，富山大学　平成 19 年 3 月 15 日～17 日

[2] 荒谷 広宣，陳 麗，岡 宏一 整流コイルを用いたベアリングレスモータの開発 電気学会 リニアドライブ・半導体電力変換合同研究会 金沢大学(金沢市，石川県) 2006.12.07～2006.12.08

[3] 荒谷 広宣，陳 麗，岡 宏一, “整流コイルを用いたベアリングレスモータの開発,” 2006.11.01～2006.11.02 第 15 回 MAGDA コンファレンス in 桐生 -電磁現象及び電磁力に関するコンファレンス-桐生市市民文化会館(桐生市，群馬県)

[4] Hironobu Aratani, Chen Li, Koichi Oka. Development of Bearingless Motors with Rectified Circuit Coil -Study of Rotation Mechanism, 2004.10.09～

2004.10.10 Dynamics & Design Conference 2004(日本機械学会).

[5] 藤原 佑輔，岡 宏一，陳 麗, “永久磁石の運動制御による鉄球の回転制御－実験による回転特性の検討,” 2006.10.26～2006.10.27, 電気学会 リニアドライブ研究会,東京電機大学(千代田区，東京都).

[6] Hironobu Aratani, Chen Li, Koichi Oka. Development of Bearingless Motors with Rectified Circuit Coil -Study of Rotation Mechanism- FAN Symposium '04 in Kochi(日本知能情報ファジィ学会) 2004.12.16～2004.12.17

[7] Yusuke Fujiwara, Cui Tianshi, Chen Li, Koichi Oka. Development of Rotation Control Mechanism for Maglev System Using Permanent Magnet,リニアドライブ・半導体電力変換合同研究会(電気学会) 2005.03.07

[8] Hironobu Aratani, Chen Li, Koichi Oka. Development of Bearingless Motors with Rectified Circuit Coil, 荒谷広宣，陳麗，岡宏一日本機械学会中四国学生会 第 35 回学生員卒業研究発表講演会(日本機械学会),.2005.03.14～2005.03.15

[9] Yusuke FUJIWARA, Cui Tianshi, Chen Li, Koichi OKA. Development of SpinningControl Mechanism for Maglev System Using Permanent Magnet and Linear Actuator,第 14 回 MAGDA コンファレンス in 岐阜-電磁現象及び電磁力に関するコンファレンス-(日本 AEM 学会) .2005.06.22～2005.06.24

[10] Yusuke FUJIWARA, Cui Tianshi, Chen Li, Koichi OKA. Manipulation by Linear Driving Permanent Magnet -Rotation Control of Ironball-第 17 回「電磁力関連のダイナミクス」シンポジウム(日本 AEM 学会)

[11] Hironobu Aratani, Chen Li, Koichi Oka. Development of Bearingless Motors with Rectified Circuit Coil -Study of Rotation Mechanism-第 17 回「電磁力関連のダイナミクス」シンポジウム(日本 AEM 学会).